

# Machine-Learning Solutions for the Analysis of Single-Particle Diffusion Trajectories

Henrik Seckler,<sup>1</sup> Janusz Szwabiński,<sup>2</sup> and Ralf Metzler<sup>1,3,\*</sup>

<sup>1</sup>*Institute for Physics & Astronomy, University of Potsdam, 14476 Potsdam-Golm, Germany*

<sup>2</sup>*Hugo Steinhaus Center, Faculty of Pure and Applied Mathematics,*

*Wrocław University of Science and Technology, Wybrzeże Wyspiańskiego 27, 50-370 Wrocław, Poland*

<sup>3</sup>*Asia Pacific Center for Theoretical Physics, Pohang 37673, Republic of Korea*

(Dated: August 21, 2023)

Single-particle traces of the diffusive motion of molecules, cells, or animals are by-now routinely measured, similar to stochastic records of stock prices or weather data. Deciphering the stochastic mechanism behind the recorded dynamics is vital in understanding the observed systems. Typically, the task is to decipher the exact type of diffusion and/or to determine system parameters. The tools used in this endeavor are currently revolutionized by modern machine-learning techniques. In this Perspective we provide an overview over recently introduced methods in machine-learning for diffusive time series, most notably, those successfully competing in the Anomalous-Diffusion-Challenge. As such methods are often criticized for their lack of interpretability, we focus on means to include uncertainty estimates and feature-based approaches, both improving interpretability and providing concrete insight into the learning process of the machine. We expand the discussion by examining predictions on different out-of-distribution data. We also comment on expected future developments.

Single Particle Tracking (SPT) refers to the observation of the microscopic motion of molecules. In 1828 Robert Brown used SPT to observe the movement of granular particles, laying the foundations of Brownian Motion [1]. After advancements in theory spearheaded by Einstein, Smoluchowski, Sutherland, and Langevin, Jean Perrin was able to give a first estimate of Avogadro's number by observing particle motion in a colloid [2]. While SPT applies mainly to observing the movement of molecules or micron-sized tracer particles [3–15], similar SPT data are also garnered in systems ranging from the movement of animals [16–18] to eye movement [19, 20] or stock dynamics [21, 22]. Understanding such trajectories and developing techniques for their analysis is thereby of vital importance in a multitude of different fields [9, 16, 17, 21, 23–26]. Mathematically such a motion is described by a random walk as introduced by Karl Pearson [27]. Here the position  $x_i$  of a particle at time  $t_i$  is obtained via a sequence of random steps  $\Delta x_i$  ( $i = 1, \dots, T - 1$ ), such that  $x_n = x_0 + \sum_{i=1}^n \Delta x_i$  ( $n = 0, \dots, T - 1$ ). In the simplest case called "Wiener process", whose steps  $\Delta x_i$  are independent and identically distributed according to  $(2\pi\sigma^2)^{-1/2} \exp(-\Delta x_i^2/[2\sigma^2])$  with constant waiting time  $t_i - t_{i-1} = \Delta t$ , will lead to a Gaussian probability density function (PDF)

$$f(x, t) = \frac{1}{\sqrt{4\pi K_1 t}} \exp\left(-\frac{x^2}{4K_1 t}\right), \quad (1)$$

where  $K_1 = \sigma^2/\Delta t$ . Due to the action of the Central Limit Theorem, the same PDF is reached as long as the increments are independent and identically distributed with finite variance and finite mean waiting time [28, 29].

In particular this entails a linear growth of the mean squared displacement (MSD) [30–32]

$$\langle x^2(t) \rangle \sim 2K_1 t. \quad (2)$$

This type of behavior is referred to as normal diffusion, the most well-known example being the aforementioned Brownian Motion as described by Einstein, Smoluchowski, Sutherland and Langevin when analyzing the motion of small particles suspended in liquids or gases [33–36].

In practice however one often observes a non-Gaussian probability density function and/or an MSD that grows non-linearly in time [5–8, 37–48]. Here we focus on the frequent case of power-law growth of the MSD,

$$\langle x^2(t) \rangle \sim 2K_\alpha t^\alpha, \quad (3)$$

referred to as "anomalous diffusion" with the anomalous diffusion exponent  $\alpha$ . A growth slower than linear ( $0 < \alpha < 1$ ) is called subdiffusive, whereas a faster than linear growth ( $\alpha > 1$ ) is referred to as superdiffusive, with the special case of ballistic motion for  $\alpha = 2$ . For such behavior to emerge, one or more of the conditions for the CLT to kick in need to be violated, as is the case when the system shows heterogeneities, long time correlations, diverging mean waiting times and/or infinite jump variance. As an example, one may consider a granular gas with a temperature changing over time, which causes non-identically distributed increments since the increment variance is temperature dependent [49, 50]. As a random walk such a motion is modeled by Scaled Brownian Motion (SBM), in which the diffusivity is time dependent [51, 52]. A diffusivity increasing with time will lead to superdiffusion, while a decreasing one will lead to subdiffusion. As another prominent example, long time correlations are often observed in biomolecules, whose crowded environments lead to strong

\*Electronic address: [rmetzler@uni-potsdam.de](mailto:rmetzler@uni-potsdam.de)

anti-correlations (viscoelastic effects), while active motion may give rise to strong correlations. Mathematically such motion is often modeled as so-called Fractional Brownian Motion (FBM) [53]. There exist plenty of other models to explain the occurrence of anomalous diffusion [54–59], apart from the mentioned SBM and FBM, we here also consider continuous-time random walk (CTRW) with random waiting times in between successive jumps [29, 60, 61], Lévy walks (LWs) [62–66] and annealed transient time motion (ATTM) [67]. We provide short descriptions of each of these models in the Supporting Information.

Since each of these models describes different physical causes for anomalous diffusion, identifying the best fitting stochastic model is an important step in unraveling the physical origin of an experimentally observed anomalous diffusion [4, 39–43, 68]. Similarly determining specific parameters attributed to each model, such as the anomalous diffusion exponent  $\alpha$  and coefficient  $K_\alpha$ , can help quantify and/or differentiate between trajectories or systems [39, 69]. Typically this task is tackled through the use of statistical observables, aiming at quantifying the expected differences between the models [47, 70–78]. However, the stochastic nature of these models in combination with the often noisy and limited experimental data can severely hinder this process, and may lead to conflicting results from different observables. For example, it has been shown that noisy data can lead to a mistaken identification as subdiffusion [74, 79].

The rising computing power of modern processors have brought along a competing approach. Machine learning (ML) has already shown wide applicability in physical chemistry [80], and is increasingly used in a variety of fields from material science [81], to medicine [82], or quantum chemistry [83]. In particular, in recent years ML has also been applied to anomalous diffusion dynamics seen in SPT data [84–87, 89]. Here the task of finding the best way to determine the underlying diffusion model and model parameters is left to machines trained on simulated trajectories, either by directly feeding into the machine the raw position data or by extracting relevant features from the trajectories first.

After shortly discussing classical methods, we here focus on the competing approaches utilizing ML, most notably those introduced during the so-called "Anomalous Diffusion (AnDi) Challenge" [87, 88]. To address the "Black Box problem" we present a deeper look into approaches including uncertainty estimates as well as those relying on extracted features. We present tests for the limits of both approaches when applied to out-of-distribution data. We conclude with a discussion on benefits, shortcomings and expected future developments of ML techniques to analyze anomalous diffusion data.

*Classical approach.* The simplest path to the anomalous exponent is given by direct calculation of the scaling exponent of the MSD, which, given an ensemble of  $N$

trajectories, is defined as

$$\langle x^2(t) \rangle = \frac{1}{N} \sum_{n=1}^N (x^{(n)}(t) - x^{(n)}(0))^2 \sim 2K_\alpha t^\alpha. \quad (4)$$

In experiments, one often relies on time-series analysis, utilizing the time averaged MSD (TAMSD),

$$\langle \overline{\delta^2(\Delta)} \rangle = \frac{1}{\mathcal{T} - \Delta} \int_0^{\mathcal{T} - \Delta} \langle [x(t + \Delta) - x(t)]^2 \rangle dt, \quad (5)$$

with observation time  $\mathcal{T}$ . As long as the system is ergodic, the TAMSD for sufficiently long  $\mathcal{T}$  will convey the same information as the MSD. However for anomalous diffusion this is often not the case, for instance, when models feature diverging mean waiting times such as CTRW or LW. This indicates that, when experimental conditions allow access to both ensemble MSD and TAMSD, the possible difference between their behavior allows one to differentiate between ergodic and non-ergodic models.

An alternative method is provided by the  $p$ -variation test [71, 90, 91]. The sample  $p$ -variation is calculated using the difference between every  $m$ th element of the trajectory,

$$V_m^{(p)} = \sum_{k=0}^{(T-1)/m-1} |x_{(k+1)m} - x_{km}|^p. \quad (6)$$

Different models often show different behavior of the  $p$ -variation. For example, for FBM we have,

$$V_m^{(p)} \propto m^{p\alpha/2-1}, \quad (7)$$

implying that, as a function of  $m$ , the  $p$ -variation increases for  $p > 2/\alpha$  and decreases for  $p < 2/\alpha$ . This is in contrast to, e.g., CTRW, where the  $p$ -variation will decrease for  $p > 2$  and increase for  $p < 2$ , regardless of anomalous exponent  $\alpha$ . Thus, calculating the  $p$ -variation for different  $p$  values can help differentiate between models or, for some models, provide an estimate of the anomalous exponent  $\alpha$ . However, static noise may compromise the  $p$ -variation output, as, e.g., tested for subdiffusive CTRWs [92]. Alternatively, it is also possible to decompose the anomalous dynamics into the Moses  $M$ , Noah  $N$ , and Joseph  $J$  scaling exponents (with  $\alpha/2 = J + L + M - 1$ ), obtained from the scaling of the cumulative absolute increments, the sum of the squared increments and the rescaled range statistic. Each of these exponents corresponds to the violation of one of the three conditions for the CLT [78, 93–95].

Another method is given through the use of the single-trajectory power spectral density (PSD) [72–74],

$$S(f, \mathcal{T}) = \frac{1}{\mathcal{T}} \left| \int_0^{\mathcal{T}} dt e^{ift} x(t) \right|^2. \quad (8)$$

Of particular interest here is the so-called coefficient of variation,

$$\gamma(f, \mathcal{T}) = \frac{\sigma(f, \mathcal{T})}{\mu(f, \mathcal{T})}, \quad (9)$$

where  $\sigma(f, \mathcal{T})$  and  $\mu(f, \mathcal{T})$  are the mean value and variance of the PSD. In FBM for example,  $\gamma(f, \mathcal{T})$  shows distinct behavior for subdiffusion ( $\gamma(f, \mathcal{T}) \sim 1$ ), superdiffusion ( $\gamma(f, \mathcal{T}) \sim \sqrt{2}$ ) and normal diffusion ( $\gamma(f, \mathcal{T}) \sim \sqrt{5}/2$ ), in the limit of high frequencies or long observation times [41]. Single-trajectory PSDs are also quite robust against static and dynamics noise [74].

The aforementioned methods cover only a fraction of possibilities, other techniques not further specified here include the use of the velocity autocorrelation [47], the first passage statistics [75], the codifference [76] or the autocovariance [77]. The applications of these statistical techniques, however, struggle when data is sparse and often require an ensemble of trajectories. For some of these methods, noisy trajectories may also present a problem, as they may lead to a erroneous identification, e.g., as subdiffusion [74, 79].

As an alternative approach to classify SPT data Thapa et al. demonstrated, that Bayesian Inference may be used to determine the best fitting model and its parameters directly from the position data of an SPT experiment using their mathematical description [96]. Specifically, these descriptions allow one to directly calculate the likelihood of a given trajectory for a specific model with given parameters. These parameters are then adjusted to maximize the probability of the trajectory. The difference in maximum likelihood is used to determine the most probable model. This method has shown great promise for processes, for which the likelihood is easily calculated in closed form, such as FBM or SBM. They struggle, however, when models feature hidden waiting times, though there have been recent advances using hidden Markov processes [97]. Even so, high computational cost remains an issue of Bayesian Inference, often resulting in a trade-off between computational feasibility and accuracy.

*The Anomalous Diffusion Challenge.* ML in recent years has grown into a strongly competing class of approaches. In 2019 Granik et al., using a convolutional neural network, demonstrated that one can differentiate between simulated Brownian motion, CTRW and sub- or superdiffusive FBM trajectories [84]. In the same year Bo et al. used a similar procedure to determine the anomalous diffusion exponent of FBM trajectories via a recurrent neural network [85]. Similarly, in 2020 Muñoz-Gil et al. demonstrated that a random tree forest can differentiate between CTRW, LW, FBM and ATTM, and provide an estimate for the anomalous diffusion exponent [86]. In all these cases, it was shown that ML can achieve better accuracy than conventional methods, especially when the available data is sparse. It should be noted, however, that these approaches all suffer from the often-quoted "Black Box problem", outputting answers without explanations as to how these are obtained [98], as detailed below.

Among ML approaches, the mentioned strategies utilizing convolutional neural networks [84, 99], recurrent neural networks [85, 89], and random tree forests [86] already differ significantly. In an effort to compare the performance of different techniques, in 2020 Muñoz-Gil et al. launched the AnDi-Challenge [87, 88]. Reported in 2021, the goal of the AnDi-Challenge was to provide a competitive comparison of different available methods to decode anomalous diffusion [87, 100]. The AnDi-Challenge also continues to serve as a benchmark to quickly assess the performance of newly developed or improved methods [94, 95, 97, 101–111].

The challenge consisted of three tasks: (i) inference of the anomalous diffusion exponent, (ii) classification of the diffusion models and (iii) segmentation of trajectories. For tasks (i) and (ii), participants were given a set of trajectories, each randomly generated from one of five different anomalous diffusion models with a randomly chosen anomalous diffusion exponent. For task (iii), the model and/or exponent changed at a given point in the trajectory. Participants were required to predict the change point in addition to the model and the anomalous diffusion exponent in both segments. To emulate experimental data, all trajectories were corrupted by white Gaussian noise of varying strength. Moderately-sized training data sets as well as the code necessary to generate further labeled data are freely available in a repository [112].

In total, 15 teams participated in the AnDi-Challenge, using a variety of different methods. While most teams used some form of ML, the more traditional approaches were represented by teams using Bayesian Inference [97, 111, 113] and scaling analysis as well as feature engineering, primarily based on a decomposition method using the Moses, Noah, and Joseph exponents [94, 95].

Several different ML techniques were used, some of which were applied to the raw position data [85, 101–105]. Others methods relied on features extracted from the input trajectories [91, 99, 106–109, 114], or used a combination of both strategies [115, 116]. The techniques using raw data focused on deep learning (DL) [84, 85, 101–105], while the feature-based methods also included other ML methods such as gradient boosting [99, 108, 114], random forests [91, 99, 108, 114], and extreme learning machines [107]. In the AnDi-Challenge the ML methods outperformed the classical approaches with top results obtained by DL, achieving an accuracy of 88% for model classification and a mean absolute error (MAE) of 0.14 for the regression of the anomalous diffusion exponent for 2D trajectories [100]. For comparison, the more traditional Bayesian Inference—with the limited amount of processes for which the likelihood function was derived at that point—achieved an accuracy of 53% and MAE of 0.20 in the challenge [100]. Classical observables such as the above-mentioned decomposition method using the scaling exponents  $M$ ,  $N$ , and  $J$ , scored 51% accuracy with an MAE of 0.31 [100].

*The raw data approach of deep learning.* Following the rising availability of high computational power along

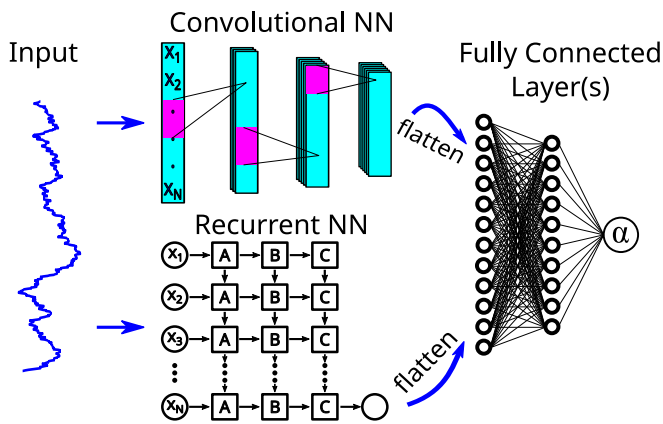


FIG. 1: Schematic representation of convolutional and recurrent neural network architectures for the analysis of single particle trajectories. In both cases input data consist of normalized trajectory positions (or increments)  $x_1, \dots, x_N$ . In a convolutional neural network a kernel is slid along the input data, generating outputs for each region. Usually each layer consists of multiple kernels with identical sizes but different weights, each generating a new data sequence depicted in the figure as an additional dimension. We here show a convolutional neural network with three layers utilizing 3, 5 and 6 kernels, respectively. In a recurrent neural network, as depicted in the lower half, the data is passed in sequence through a recurrent unit, with the output of the previous time step included as input in the next step (vertical connections in the figure). Here we depict a stacked recurrent neural network consisting of three layers with weight matrices  $A, B, C$  respectively. For both recurrent and convolutional networks the resulting output is usually flattened into a one-dimensional array and passed through one or multiple fully connected layers, ending, e.g., in a prediction of the anomalous diffusion exponent  $\alpha$  or diffusion coefficient  $K_\alpha$ .

with increasingly more detailed data sets, more and more ML approaches rely on highly complex architectures involving thousands of parameters. With DL we refer to neural networks with many hidden layers, often resulting in several hundreds of thousand of fitting parameters (weights) [117]. The complexity of these models allows them to directly learn from massive amounts of raw data, with little to no need for human-engineered preprocessing. Specifically for the analysis of anomalous diffusion, this entails directly learning from the position time series of the recorded trajectories. To speed up training and reduce the required data volume, the input data will undergo minimal preprocessing, via a normalization of its standard deviation. Since diffusion models only rely on the increments of a process and no additional relevant information is included in the absolute positions, the trajectories are often also converted to the increment process [85, 101–105, 112]. In inhomogeneous, static environments, this condition may, of course, no longer hold.

The DL solutions, as presented in the AnDi-Challenge and newly developed ones since, mostly utilize convolutional [84, 102–105] and recurrent [85, 101, 102, 118] neural network architectures. In convolutional neural net-

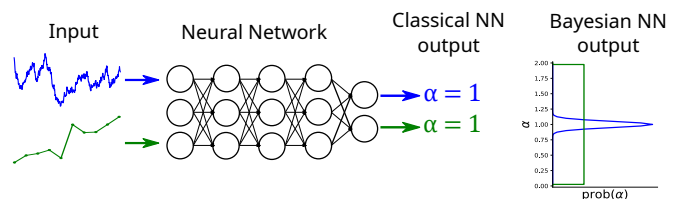


FIG. 2: Uncertainty problem of DL. The same anomalous diffusion exponent is predicted for two trajectories of different length, when fed into a classical neural network—despite their differing amount of information. The two cases can only be distinguished when the probability distribution of possible output anomalous diffusion exponents is considered, instead of a point estimate. Such an estimate can be provided by Bayesian neural networks. Figure adapted from [110].

works, best known for their applications in image classification, the layers consist of one or several convolutional kernels that are slid along the input tensor [119]. By stacking multiple such layers, they are able to detect correlations in the sequence. Recurrent neural networks, most notably the so called "long short-term memory" (LSTM) networks, are specifically designed for time sequence data, making them useful for tasks such as speech recognition, translation, or sequence forecasts [120]. Layers typically consist of a single recurrent unit applied successively to each time step, with outputs of the previous time step included as additional inputs for the next time step. Figure 1 shows simplified schematic representations of both architectures. Other notable architectures that have been shown to be applicable to single particle tracking data analysis include graph neural networks [115, 116] and transformer/encoder networks [103, 104].

In the AnDi-Challenge all top results were achieved by DL [84, 100–103, 106], though notably one of these did rely on extracted features rather than the raw trajectories [106]. Overall, DL, and ML in general, showed great promise in the community challenge. However, one should not dismiss the shortcomings of such methods, which are most often criticized for their lack of interpretability [98]. To that end, we discuss added uncertainty estimations as well as feature-based approaches in the following.

*Qualifying deep learning by including uncertainties.* Classical DL models only provide point estimates of the output and do not furnish any concrete information on the reliability of this estimate. In extreme cases, this also means that these methods will provide outputs on data, that have nothing to do with the learned problem. Even within the desired task, different inputs may provide the same point estimate, but underlie massively different uncertainties. As an example, figure 2 depicts two diffusion trajectories, which, fed into a neural network, would both be assigned an anomalous diffusion exponent of  $\alpha = 1$ , even though one input contains considerably more information (data points) than the other. To reveal the difference, one would need to output a probability distribution of  $\alpha$  values instead. Examining such a distri-



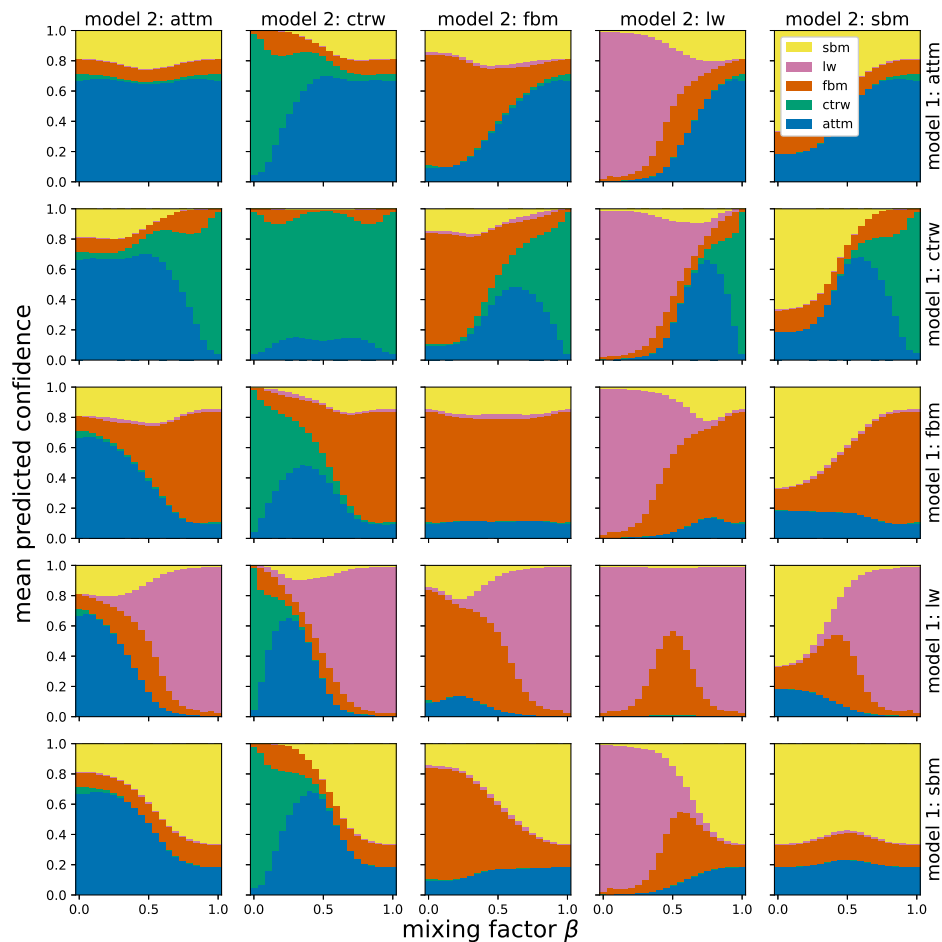


FIG. 3: ML-classification for a superposition of 2 models. The panels depict the mean confidence assigned by the neural network, when presented with a mixture of two models in dependence of the mixing factor  $\beta$ . The depicted results are obtained from two-dimensional trajectories with 100 data points each.

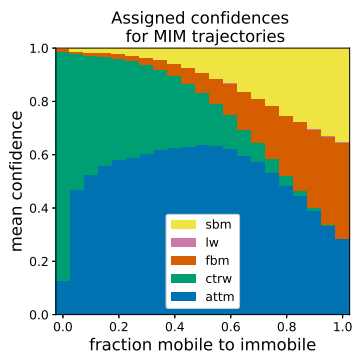


FIG. 4: Classification for Mobile-Immobile-Model trajectories for different fractions of mobility. The MIM effectively converges to CTRW for low mobile fractions  $f_m$ , and to Brownian motion for  $f_m \approx 1$ . The depicted results are obtained from one-dimensional trajectories with 250 data points each.

bution reveals that, while the first trajectory is roughly a Brownian motion, the prediction of the second is just

the result of obtaining no relevant information, with the uniform distribution  $\alpha \in [0, 2]$  leading to a point estimate of  $\alpha = 1$ .

To change the predictions to a probability distribution, we need to model two types of uncertainty [121, 122]. *Aleatoric* uncertainty refers to the uncertainty inherent in the data, caused, for instance, by measurement noise or an inherent stochasticity of the system. This uncertainty remains even for a perfect model obtained from an infinite amount of data and therefore must be included in the output of the neural network model and trained by utilizing an appropriate loss function [123, 124]. As no model is perfect, it is insufficient to consider aleatoric uncertainty alone. Namely, to account for the difference between training and test data, or an insufficient amount of training data in the first place, one needs to introduce a second uncertainty measure. *Epistemic* (or *systematic*) uncertainty can be included by considering the weights of the neural network themselves as uncertain quantities. Formally, the probability  $p(\theta|\mathcal{D})$  of the weights  $\theta$ , given

data  $\mathcal{D}$ , is given by Bayes' rule [125],

$$p(\theta|\mathcal{D}) = \frac{p(\mathcal{D}|\theta)p(\theta)}{p(\mathcal{D})}. \quad (10)$$

To obtain the final probability  $p(y|x_i, \mathcal{D})$  for some output  $y$  given the input  $x_i$ , we combine the aleatoric uncertainty, represented by the probability  $p(y|x_i, \theta)$  for one set of weights  $\theta$ , with the epistemic uncertainty by marginalization over the weights. The resulting integral is usually approximated through Monte Carlo sampling [126, 127],

$$\begin{aligned} p(y|x_i, \mathcal{D}) &= \int d\theta p(y|x_i, \theta)p(\theta|\mathcal{D}) \\ &\approx \frac{1}{M} \sum_{m=1}^M p(y|x_i, \theta_m), \end{aligned} \quad (11)$$

where  $\theta_m$  is sampled from the distribution  $p(\theta|\mathcal{D})$  for a sufficient number  $M$  of discrete points. As an exact calculation of  $p(\theta|\mathcal{D})$  (via equation 10) quickly becomes computationally infeasible for deep neural networks, one uses approximations to generate the samples  $\theta_m$ . Various methods, summarized under the term *Bayesian Deep Learning*, have been proposed, the simplest of which is to train an ensemble of neural networks, known as *deep ensembles* [128]. Other ways to generate samples include *MC-Dropout* [129, 130], in which one uses dropout to generate multiple samples from the same neural network, and *Stochastic Weight Averaging Gaussian* (SWAG) [131, 132], which approximates  $p(\theta|\mathcal{D})$  by a Gaussian distribution, obtained by interpreting a stochastic gradient descent [133] as an approximate *Bayesian Inference* scheme.

Recently it was demonstrated that based on *Multi-SWAG*, a combination of SWAG and deep ensembles, one can add informative uncertainty predictions to the DL solution for the analysis of single-particle anomalous diffusion trajectories [110]. The introduced method maintains the performance of the top AnDi-Challenge competitors, while it provides a well calibrated uncertainty estimate with expected calibration errors [134, 135] of only 0.0034 for the regression of  $\alpha$  and 0.45% for the classification of the diffusion model. On top of this, it was demonstrated [110] that the added error prediction improves the interpretability of the deep neural networks, demonstrating in detail that the predicted behavior can be linked to properties of the underlying diffusion models. In the Supplementary figure S1 an example is shown of how error predictions can be analyzed when inferring the anomalous diffusion exponent.

To further elaborate on the study in [110], we now discuss the results obtained from the Multi-SWAG approach when confronting the introduced networks with previously unseen out-of-distribution data. First, we examine the outputs when feeding the network with a superposition of two models, the increments of which are obtained by the weighted sum of the increments of two models

with random anomalous diffusion exponents. With the mixing factor  $\beta$  we then obtain

$$\Delta x_{\text{new}} = \beta \Delta x_{\text{model1}} + (1 - \beta) \Delta x_{\text{model2}}. \quad (12)$$

Based on two-dimensional trajectories of length 100, figure 3 shows the mean confidences, that is, the mean value of the predicted model probabilities over  $2 \times 10^5$  input trajectories, in dependence of the mixing factor for different model combinations, represented by the rows and columns in the panel grid. For the convenience of the reader, the panels include the redundant case of swapped model 1 and 2, which results in a symmetry with respect to the panel grid diagonal, i.e., superpositions of a model with itself. In most cases we see a smooth transition of the confidence from the marginal cases on the left and right, which are the normal predictions for pure trajectories of model 2 and 1, respectively. A notable exception, however, is the behavior for superpositions with CTRW, as these often show high probabilities for ATTM. Since ATTM could be considered a combination of CTRW and Brownian motion, often showing the jumping motion of CTRW interspersed with Brownian motion, this is not unexpected. Moreover, we see that superpositions with LW often show high probabilities for FBM, which can be explained due to the similarity of LW with highly correlated FBM. Analogous behavior can be seen in 1D in the Supplementary figure S2.

As another example we confront the trained neural network with trajectories obtained from the "Mobile-Immobile-Model" (MIM) [136–138]. In the MIM, trajectories switch between a mobile and an immobile state, with mean residence times  $\tau_m, \tau_{im}$ . At equilibrium the fraction of time a test particle spends in the mobile phase is given by  $f_m = \tau_m / (\tau_m + \tau_{im})$ . This model provides information about the immobilized fraction of the particle motion. Moreover, it includes a continuous transition between a normal-diffusive ( $\alpha = 1$ ) CTRW on the one side, for a low fraction of the mobility ( $f_m \rightarrow 0$ ), and Brownian motion on the other side, for a high fraction of the mobility ( $f_m \rightarrow 1$ ). The results, depicted in figure 4, confirm that the method correctly classifies the two extremes as CTRW for low mobility and as Brownian motion for high mobility, which for this method is represented as a split probability between SBM, FBM and ATTM (all three models that can exhibit Brownian motion). In between these two limits we see high confidences for ATTM, which is not surprising, as ATTM is the only model, of those considered here, that mimics the phase switching behavior of a MIM trajectory.

*Feature-based classification of single particle trajectories.* As demonstrated by the AnDi-Challenge [100], DL methods perform excellently in the analysis of the diffusion models and outperform the more traditional approaches to single particle tracking data. However, the choice of a suitable classification method is usually more subtle than simply looking at its performance. The availability of tools and libraries for DL makes it relatively easy to quickly create effective predictive models. But

due to their complexity, those models are Black Boxes providing (almost) no insight into the decision making processes. In the previous section we showed how confidences can be established to judge the validity of the provided output. Here we consider the interpretability of the parameters in the ML approach. To give an example for the complexity in DL consider ResNet18, one of the simplest deep residual network architectures used in [89] for trajectory classification. This network originally had 11,220,420 parameters. The authors were able to reduce this number down to 399,556 with a positive impact on accuracy of the resulting classifier. Although this is an impressive achievement, the interpretation of all those remaining parameters is, of course, practically elusive.

The tradeoff between model accuracy and its interpretability is one of the reasons for feature-based attempts for the classification of diffusion models [86, 91, 99, 108, 114, 139]. These feature-based methods are statistical learning algorithms that do not operate on raw data. Instead, each data sample is characterized by a vector of human-engineered features or attributes. Those vectors are then used as input for a classifier (see figure 5 for a workflow of the method). In some sense, those methods may be treated as a kind of extension to the statistical techniques usually used for classification purposes. Instead of conducting a testing procedure based on one statistics, we can turn all of them into features and use them to train the model. This could be of particular importance in situations, when single statistics yield inconclusive results or when testing results based on different statistics significantly differ from each other [87]. Automated feature-based analysis can thus be used in addition to deep learning methods to learn more about the values of specific features and their relative importance in categorizing input data.

Feature engineering, i.e., the process of extracting attributes from raw data, is not a trivial task. It requires domain expertise to pinpoint which features may be valuable for the process that generated the given set of data. It may also be time and resource consuming, as testing the impact of newly created features on the predictions involves repetitive trial and error work. It has been already shown [99] that classifiers, which were trained with a popular set of features, may not generalize well beyond the situations encountered in the training set. Thus, careful attention needs to be paid to the choice of the attributes. They should cover all important characteristics of the process, but, at the same time, they should contain the minimal amount of unnecessary information, as each redundant piece of data causes noise in the classification and may lead to overfitting (see [141] for a general discussion concerning the choice of features).

Once the appropriate set of features is identified, the choice of an actual classification algorithm is of secondary importance. Very often, random forest [86, 91, 99, 114, 139] or gradient boosting [86, 91, 99, 108, 114] methods are used, because they offer a reasonable compromise be-

tween the accuracy of the results and their interpretability. Both algorithms fall into the category of ensemble learning, i.e., methods that generate many classifiers and aggregate their results. In both cases, decision trees [142] are used as the basic classifier. In a random forest, several trees are constructed from the same training data. For a given input, the predictions of individual trees are collected and then their mode is taken as the output. In case of gradient boosting, the trees are not independent. Instead, the single classifiers are built sequentially from the mistakes committed by the ensemble (see figure 6). In terms of interpretability, both algorithms are placed between single decision trees (that are easy to interpret) and DL (with the Black Box problem).

In the AnDi-Challenge, the feature-based contribution was outperformed by the winning teams using DL (73% accuracy versus 88% for the winners). However, the authors of the feature-based method further elaborated on their set of features to achieve 83% accuracy on the same validation set [108]. This was based on a mixture of characteristics tailor-made to the diffusion processes (e.g., MSD, anomalous diffusion exponent, diffusion coefficient) and problem-agnostic ones (e.g., detrending moving average, kurtosis). All features used in [87] and [108] are summarized in table I.

The authors were able to assess the importance of the features in the overall classification and to calculate the contribution of each attribute to the classification of every single trajectory, giving some insight into the decision making process of the classifier [108]. The results achieved with a simple gradient boosting method indicate that the feature-based ML, overshadowed somewhat by DL approaches in the recent years, constitutes a serious alternative to the state-of-the-art approaches. It should be also mentioned that better interpretability is not the only benefit related to feature-based methods. Compared to DL, they usually work better on small data sets and are computationally (and thus also financially) cheaper, see [99] for a short comparison. Additionally, in case of single particle tracking data, they naturally allow for the simultaneous analysis of trajectories of different lengths.

*Testing the limitations of machine learning.* During the AnDi-Challenge the competitors were provided with large training data sets and tested on data generated from the same distributions as used for the training. This practice gives an undeniable advantage to ML in general and DL especially. Additionally the artificial data used in the AnDi-Challenge only considered white Gaussian noise, which may not be sufficient to account for all the noise sources present in experimental data. To address these problems we here test ML models to analyze their performance when confronted with (a) data corrupted with dynamic noise and (b) the task of determining the anomalous exponent for models not included in the training data. These tests should indicate (a) how robust the methods are to different noise types and (b) how well the learned determination of  $\alpha$  can be generalized to other

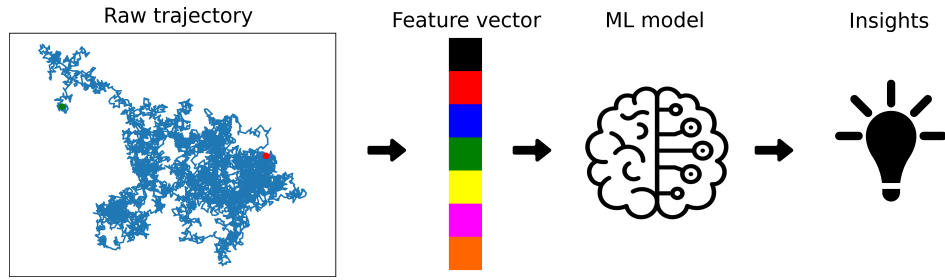


FIG. 5: Schematic workflow of the feature-based method: a set of features is extracted from raw trajectories and used as input to the classification or regression model. Analysis of the impact of the features on the outcome give insights into the decisionmaking process of the model.

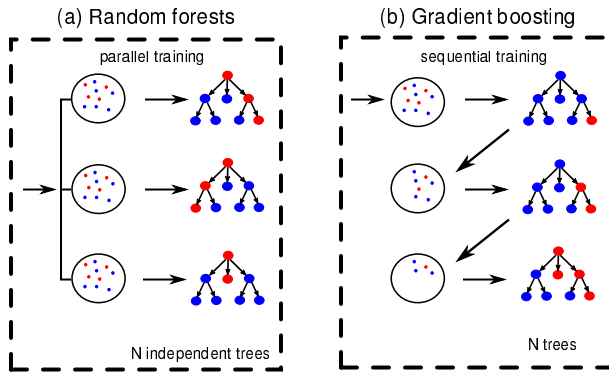


FIG. 6: Schematic comparison between random forest (left) and gradient boosting methods (right). In the random forest,  $N$  independent trees are built in parallel from random subsets of the input data set. In gradient boosting, the next tree is constructed from the residuals of the ensemble and added to it.

models.

Dynamic noise stems from the finite exposure time needed to generate each data point. In contrast to the additive Gaussian white noise this error is characterized by temporal integration, which for discrete time steps is replaced by a sum,

$$\bar{x}(t) = \frac{1}{\tau_e} \int_0^{\tau_e} x(t - \xi) d\xi \rightarrow \frac{1}{n_e} \sum_{j=0}^{n_e-1} x(t - j\Delta t), \quad (13)$$

where  $\tau_e = n_e \Delta t$  is the exposure time consisting of  $n_e$  time steps of length  $\Delta t$  [74, 143]. To test the ML models we generate data sets, in the same manor as in the AnDi-Challenge, but with added dynamic noise of different exposure times containing 10,000 trajectories each. In table II we see the results when confronting the DL model introduced in [110] and a feature-based model utilizing the features from [108] with data corrupted by dynamic noise. For DL, the determination of the anomalous exponent seems to be robust to the influence of dynamic noise, only resulting in a slight performance decrease from an MAE of 0.207 to 0.235 with increasing dynamic noise as characterized by exposure time steps  $n_e$ , considering that a slight performance loss with higher noise is to

$n_e = 20$   
total accuracy: 53.49%

Predicted model \ True model	attn	ctrw	fbm	lw	sbm
attn	0.59	0.41	0.086	0.075	0.1
ctrw	0.17	0.55	0.002	0.0015	0.003
fbm	0.1	0.015	0.73	0.69	0.2
lw	0.005	0	0.0095	0.12	0.0065
sbm	0.14	0.019	0.18	0.12	0.69

FIG. 7: Confusion matrix for dynamic noise with  $n_e = 20$  for the DL model introduced in [110]. While FBM, ATTM and SBM show similar behavior to the case without dynamic noise, identification of CTRW and especially LW is strongly compromised by dynamic noise.

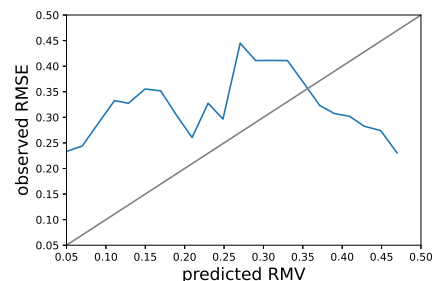


FIG. 8: Confidence Accuracy diagram obtained when trying to apply the DL model from [110] to the elephant random walk. We see a strong deviation between predicted root mean variance and observed root mean squared error, indicating that the learning error prediction from the other models does not translate well to the elephant random walk.



<b>Original features</b>	
Anomalous exponent	
Diffusion coefficient	
Asymmetry	
Efficiency	
Empirical velocity autocorrelation function	
Fractal dimension	
Maximal excursion	
Mean maximal excursion	
Mean Gaussianity	
Mean-squared displacement ratio	
Kurtosis	
Statistics based on $p$ -variation	
Straightness	
Trappedness	
<b>Additional features</b>	
D'Agostino-Pearson test statistic	
Kolmogorov-Smirnov statistic against $\chi^2$ distribution	
Noah exponent	
Moses exponent	
Joseph exponent	
Detrending moving average	
Average moving window characteristics	
Maximum standard deviation	

TABLE I: Features used to characterize single particle trajectories. The original set of features was used in the AnDi-Challenge and achieved 73% accuracy. With the additional features, the performance of the classifier increased to 83%. The definitions of the features may be found in Appendix B and in [108].

dynamic noise $n_e$	MAE		accuracy	
	DeepL	feature	DeepL	feature
1	0.207	0.23	78%	71%
2	0.221	0.23	69.8%	71%
5	0.229	0.22	59.3%	68%
10	0.232	0.22	55.2%	65%
20	0.235	0.22	53.5%	65%

TABLE II: Performance of ML models, when confronted with data corrupted by dynamic noise of different strength, as characterized by the exposure length  $n_e$ . The case  $n_e = 1$  corresponds to no dynamic noise. The table shows the performance for the DL-based method introduced in [110] as well as a feature-based method utilizing the features introduced in [108].

	MAE	
	NN50	NN200
deep learning model	0.246	0.264
feature-based model	0.348	0.318
trained on subset of NN50	0.196	0.175
trained on subset of NN200	0.197	0.166

TABLE III: Performance of ML models when confronted with data generated from the elephant random walk (ERW). The two cases NN50, NN200 correspond to ERW, when one takes every 50th or 200th data point. The table shows the accuracy for the DL-based method introduced in [110] as well as a feature-based method utilizing the features introduced in [108]. For reference the table also shows what performance can be achieved, when the feature-based model is trained on a subset of the ERW test data in the last two rows.

be expected. The model does however seem to struggle with classification for high dynamic noise, where the accuracy drops from 78% down to 53.5% for the highest considered dynamic noise  $n_e = 20$ . A look at the confusion matrix in figure 7 reveals that this is caused by miss-classification of LW and CTRW, evidently the added Gaussian noise in the training data is not sufficient to account for the changes incurred by dynamic noise. The feature-based model proves more robust to the influence of dynamic noise, showing a constant MAE of  $\approx 0.22 - 0.23$ , slightly outperforming the DL model for high dynamic noise. Even more striking are the results obtained for classification, while starting with a worse accuracy than DL ( $\approx 71\%$  compared to  $\approx 78\%$ ), the feature-based model turns out to be much less hampered by high dynamic noise levels, only decreasing the accuracy to  $\approx 65\%$  (compared to  $\approx 53.5\%$  for DL) at the highest noise level. Critically, when dealing with experimental setups with high dynamic noise, for accurate classification, dynamic noise should therefore be included in the training data sets, especially when relying on a DL model.

The elephant random walk (ERW) is a process with infinite memory, according to which the next position of the walker is given by

$$x_i = x_{i-1} + \sigma_i, \quad (14)$$

with the random variable  $\sigma_i = \pm 1$  [144]. The choice of  $\sigma_i$  is determined through the memory of the previous time steps, by first drawing a random integer  $0 \leq j < i$  and then choosing  $\sigma_i = \sigma_j$  with probability  $p$  or  $\sigma_i = -\sigma_j$  with probability  $1 - p$ . The first step  $\sigma_0$  is given as  $\sigma_0 = 1$  with probability  $q$  or  $\sigma_0 = -1$  with probability  $1 - q$ , for this work we choose  $q = 1/2$ . In [144] it was shown that, in the limit of many steps, this leads to the long time

behavior of the MSD,

$$\langle x^2(t) \rangle \simeq \begin{cases} \frac{t}{3-4p}, & p < 3/4 \\ t \ln(t), & p = 3/4 \\ \frac{t^{4p-2}}{(4p-3)\Gamma(4p-2)}, & p > 3/4, \end{cases} \quad (15)$$

which corresponds to normal diffusion for  $p < 3/4$  and superdiffusion for  $p > 3/4$  with  $\alpha = 4p - 2$ . We generate a data set containing 10,000 trajectories of length  $T = 100$ , uniformly distributed in  $\alpha \in 1, 1.05, \dots, 2.0$ , where for  $\alpha = 1$  we choose a  $p < 3/4$  randomly. To eliminate peculiarities caused by the constant step size, and to provide sufficiently many steps to observe long time behavior (15) of the MSD, we only take every  $NN = 50$ th or  $NN = 200$ th data point, effectively generating trajectories of length 5,000 or 200,000 and shortening them to length 100, plus corrupting them with white Gaussian noise. The results when confronting the models with this data set are listed in table III. For the DL model introduced in [110] with this data set, we achieved an MAE of  $\approx 0.246$  (for  $NN = 50$ ). While this is a significant improvement from an unknown prediction of  $\alpha \in [0.05, 2]$  (MAE of  $\approx 0.49$ ), which the model was trained on, it does not improve much on the performance expected when only identifying the elephant random walk as superdiffusive with  $\alpha \in [1, 2]$  (MAE of  $\approx 0.25$ ). In addition, when considering the uncertainty predictions, that are provided by the method as well, we find that the predictions learned on different models are of little to no use when transferred to the elephant walk. Depicted in figure 8, we see that the predicted and observed errors differ significantly. A possible reason for this can be found by closer inspection of the predicted anomalous diffusion exponent, which reveals that an unusually high number of trajectories are predicted at, or close to, a ballistic motion with  $\alpha = 2$  (31% of trajectories are predicted with  $\alpha \geq 1.9$  as compared to 9,5% with a true  $\alpha \geq 1.9$ ). This might be caused by the elephant random walk—on a single trajectory basis in the superdiffusive regime—featuring a drift that only gets eliminated in the ensemble average. Detecting this drift, while not specifically being trained to deal with it, might lead the model to a falsely confident prediction of ballistic motion. For the feature-based model in table III we achieved only an MAE of  $\approx 0.348$  or  $\approx 0.318$  for  $NN = 50$  or  $NN = 200$  respectively. For reference we here also included the results one can obtain when training the feature-based model on subsets of the ERW data sets. These indicate what performance could be expected with appropriately trained models achieving an MAE of  $\approx 0.196$  (for  $NN = 50$ ) and  $\approx 0.166$  (for  $NN = 200$ ), and thereby significantly improving on the performance of the models trained on the data sets of the AnDi-Challenge. In conclusion we see that while some information can be extracted, for accurate predictions, the machine needs to be trained on the appropriate model.

It should be noted however, that classical methods such as Bayesian Inference, would similarly struggle when

applied to a wrong prior, likely resulting in falsely confident predictions as well. Likewise, it is known that not considering a specific type of noise can lead to wrong predictions when using statistical observables [74]. Nevertheless, it is important to stress that ML does not circumvent the necessity to consider such cases and should be applied appropriately.

*Outlook.* The results of the AnDi-Challenge proved the potential of ML approaches when analyzing anomalous diffusion data. They come, however, at some price, often acting as a Black Box, providing answers without explanation. This lack of explainability limits their usefulness when applied to real-world problems and, inter alia, can lead to some overconfidence in the output results. Building on the AnDi-Challenge we here presented two methods, which improve the machine’s explainability.

Extracting a set of statistical features, instead of using the raw position data, allows us to use easier to interpret ML algorithms. In addition, one can determine the importance of each feature, further improving interpretability. In a recent publication, Mangalam et al. propose multifractal features in order to improve the classification of anomalous diffusion [145] which will be examined in future publications. As an alternative to the trade-off brought by feature-based methods, we can include an uncertainty prediction in the output of deep neural networks, using the Multi-SWAG Bayesian DL method on top of the ML algorithm, at no cost of accuracy. Apart from the obvious use of an added reliability estimate, an analysis of these error predictions offers additional insights into the learning process of the machine. Note that this method could also be applied to feature-based DL approaches and that similar techniques for gradient boosting or random forest algorithms exist [146]. Despite these improvements, we showed that these methods can still be hampered by out-of-distribution test data, such as noise or models not included in the training data, possibly leading to overconfident predictions due to the misspecified prior. To judge the validity of ML outputs and prepare appropriate training data sets, analysis of experimental data using statistical methods remains necessary. Moreover, we emphasize that visual inspection as well as some intuition on the system will always present another layer of confidence, or caution.

Recent work has shown that sequence to sequence models are appropriate to deal with trajectories changing between different diffusion models and/or diffusion exponents [147, 148], as was the target of the third task of the AnDi-Challenge. Extending such models to include error estimates will be a subject of future work. As an example we show the results of a preliminary model, trained on trajectories with a single change point, in figure 9. Apart from its use for uncertainty estimation, the included error output can improve the extraction of change points from the sequence, especially in cases where the anomalous diffusion exponents before and after the change point are similar, inhibiting the determination of change points

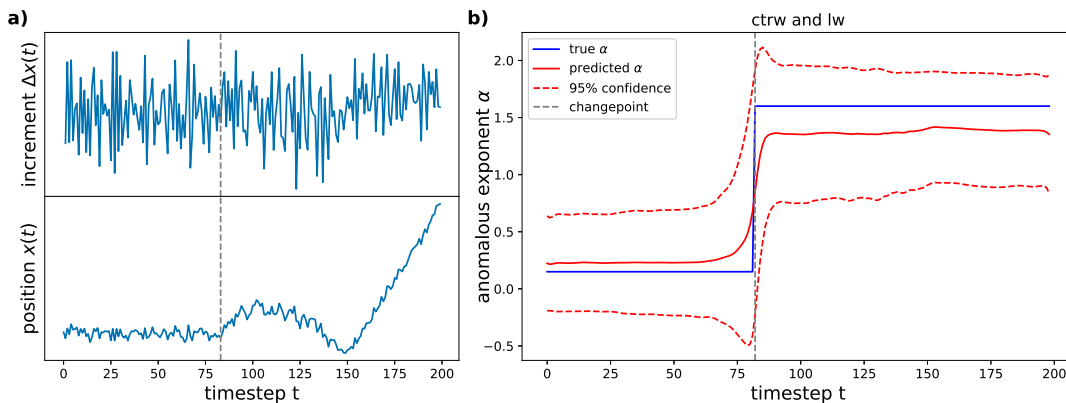


FIG. 9: Example of a sequence to sequence prediction for a trajectory with a single change point. The trajectory shown in (a) changes from CTRW with  $\alpha = 0.15$  to LW with  $\alpha = 1.60$  at time step  $t_{\text{change}} = 83$ . Panel (b) shows the output when feeding the case (a) into a trained neural network. The used model includes an uncertainty estimation, whose 95% confidence interval is indicated by the red dashed line in the figure. Note that the predicted error spikes at the change point.

only by means of the mean predictions.

Similarly to the example of superpositions of diffusion models used here, in a recent work, Muñoz-Gil et al. apply unsupervised learning to anomalous diffusion, where different neural networks are trained to reproduce trajectories generated from a specific diffusion model for each network. They show that the differing performance in reproduction, when applied to different diffusion models than trained on, can be used to classify a single, or a superposition of, diffusion model(s) [149].

On another note, as we saw in figure 2, predictions on very short trajectories tend to gravitate toward the center of the prior distributions. This will limit the usefulness of single-trajectories analysis when applied to experimental data consisting of many short trajectories. Exploring the applicability of ML techniques to these kinds of data may provide an interesting research avenue in the future, see also the approach in [118].

The application of ML, and its comparison to conventional methods, to trajectory ensembles as well as trajectories with changing diffusion models will be subject of the impending 2nd AnDi-Challenge. In addition this challenge will include video tracks of diffusing single particles, without direct access to the positions of the tracers, thereby serving as an exploration of noise-types different from the simple white Gaussian type, inherent to the conversion from video tracks to particle trajectories.

Recent advances in computer vision could open a new track of research on anomalous diffusion identification. The idea is quite simple: instead of looking for custom neural network architectures for identification purposes or preparing a robust set of features, one could (at least theoretically) turn trajectories into images and feed them into well established pre-trained computer vision models, that are known to excel in object recognition. The main difficulty with this approach is that one cannot simply take a plot of a trajectory as the image, since in this case the temporal structure of the data is lost. Hence, one

needs image representations of trajectories that retain the existing spatial and temporal relations.

First approaches utilizing the computer-vision approach are very promising. For instance, Garibo-i-Orts et al. [150] used Gramian angular fields to encode trajectories as images and two well-established pre-trained computer vision models (ResNet and MobileNet) for both classification of diffusion types and inference of the anomalous diffusion exponent  $\alpha$ . Their results for short trajectories already outperform the state-of-the-art-methods. Markov transition fields [151] or recurrence plots [152] are other candidates for trajectory imaging methods that could potentially improve the performance of the classifiers. One of the benefits of the computer vision approach is that it allows to use pre-trained models, which are available in popular DL libraries like for instance *Keras*. In other words, it makes the analysis accessible to researchers lacking an extensive background in ML.

### Author information

*Henrik Seckler* studied physics at the University of Potsdam, Germany, where he is currently pursuing his doctorate. His research interests include machine learning, data assimilation and anomalous diffusion.

*Janusz Szwabiński* obtained his BSc in Physics from University of Wrocław, Poland, and his PhD in Science from Saarland University in Saarbruecken, Germany. He is currently a university professor in the Department of Applied Mathematics at the Wrocław University of Science and Technology. He is mainly interested in complex systems and has a track record in multidisciplinary research, with applications in statistical physics, biology, social science and economy.

*Ralf Metzler* studied physics and obtained his PhD at the University of Ulm, Germany. After postdoc po-

sitions at Tel Aviv University and MIT he held faculty positions at NORDITA (Nordic Institute for Theoretical Physics, Copenhagen, Denmark), University of Ottawa, Canada, and Technical University of Munich, Germany. Ralf is chair professor in Theoretical Physics at University of Potsdam. Among his distinctions, Ralf received a Finland Distinguished Professorship from the Finnish Academy, an Alexander von Humboldt Polish Honorary Research Scholarship, and the 2017 SigmaPhi Prize. Ralf's research interest are in non-equilibrium statistical physics and stochastic processes in complex systems, soft and bio matter, and data assimilation.

### Supporting Information

Supporting Information: Definition of anomalous diffusion models, summary of trajectory characteristics for

the feature-based analysis, and supplementary figures S1 and S2.

### Acknowledgments

HS thanks Timo J. Doerries for the implementation of the MIM model. JS was supported by NCN-DFG Beethoven Grant No. 2016/23/G/ST1/04083. RM acknowledges funding from the German Ministry for Education and Research (NSF-BMBF project STAXS).

### Competing interests

The authors have no competing interests to declare.

---

### References

- [1] Brown, R. brief account of microscopical observations made in the months of june, july and august 1827, on the particles contained in the pollen of plants; and on the general existence of active molecules in organic and inorganic bodies. *Philos. Mag.* **1828**, *4*, 161-173.
- [2] Perrin, J. Brownian movement and molecular reality. *Ann. Chim. Phys.* **1909**, *18*, 5-114.
- [3] Elf, J.; Barkefors, I. Single-molecule kinetics in living cells. *Ann. Rev. Biochem.* **2019**, *88*, 635-659.
- [4] Cherstvy, A. G.; Thapa, S.; Wagner, C. E.; Metzler, R. Non-Gaussian, non-ergodic, and non-Fickian diffusion of tracers in mucin hydrogels. *Soft Matter* **2019**, *15*, 2526-2551.
- [5] Höfling, F.; Franosch, T. Anomalous transport in the crowded world of biological cells, *Rep. Prog. Phys.* **2013**, *76*, 046602.
- [6] Horton, M. R.; Höfling, F.; Rädler, J. O.; Franosch, T. Development of anomalous diffusion among crowding proteins. *Soft Matter* **2010**, *6*, 2648-2656.
- [7] Jeon, J.-H.; Tejedor, V.; Burov, S.; Barkai, E.; Selhuber-Unkel, C.; Berg-Sørensen, K.; Oddershede, L.; Metzler, R. In vivo anomalous diffusion and weak ergodicity breaking of lipid granules. *Phys. Rev. Lett.* **2011**, *106*, 048103.
- [8] Leijnse, N.; Jeon, J. H.; Loft, S.; Metzler, R.; Oddershede, L. B. Diffusion inside living human cells. *Eur. Phys. J. Spec. Top.* **2012**, *204*, 377a.
- [9] Codling, E. A.; Plank, M. J.; Benhamou, S. Random walk models in biology. *J. R. Soc. Interface* **2008**, *5*, 813-834.
- [10] Gurtovenko, A. A.; Javanainen, M.; Lolicato, F.; Vattulainen, I. The devil is in the details: what do we really track in single-particle tracking experiments of diffusion in biological membranes? *J. Phys. Chem. Lett.* **2019**, *10*, 1005-1011.
- [11] Roberts, T. D.; Yuan, R.; Xiang, L.; Delor, M.; Pokhrel, R.; Yang, K.; Aqad, E.; Marangoni, T.; Trefonas, P.; Xu, K.; Ginsberg, N. S. Direct correlation of single-particle motion to amorphous microstructural components of semicrystalline poly(ethylene oxide) electrolytic films. *J. Phys. Chem. Lett.* **2020**, *11*, 4849-4858.
- [12] Erimban, S.; Daschakraborty, S. Fickian yet non-Gaussian nanoscopic lipid diffusion in the raft-mimetic membrane, *J. Phys. Chem. B* **2023**, *127* 4939-4951.
- [13] Javanainen, M.; Martinez-Seara, H.; Metzler, R.; Vattulainen, I. Diffusion of integral membrane proteins in protein-rich membranes. *J. Phys. Chem. Lett.* **2017**, *8*, 4308-4313.
- [14] Winkler, P. M.; Regmi, R.; Garcia-Parajo, M. Optical antenna-based fluorescence correlation spectroscopy to probe the nanoscale dynamics of biological membranes. *J. Phys. Chem. Lett.* **2017**, *9*, 110-119.
- [15] Spillane, K. M.; Ortega-Arroyo, J.; de Wit, G.; Eggeling, C.; Ewers, H.; Wallace, M. I.; Kukura, P. High-speed single-particle tracking of GM1 in model membranes reveals anomalous diffusion due to interleaflet coupling and molecular pinning. *Nano Lett.* **2014**, *14*, 5390-5397.
- [16] Okubo, A. Dynamical aspects of animal grouping: swarms, schools, flocks, and herds. *Adv. Biophys.* **1986**, *22*, 1-94.
- [17] Vilck, O.; Aghion, E.; Avgar, T.; Beta, C.; Nagel, O.; Sabri, A.; Sarfati, R.; Schwartz, D. K.; Weiss, M.; Krapf, D.; Nathan, R.; Metzler, R.; Assaf, M. Unravelling the origins of anomalous diffusion: from molecules to migrating storks. *Phys. Rev. Res.* **2022**, *4*, 033055.
- [18] Bartumeus, F.; da Luz, M. G. E.; Viswanathan, G. M.; Catalan, J. Animal search strategies: a quantitative random-walk analysis. *Ecology* **2005**, *86*, 3078-3087
- [19] Engbert R; Mergenthaler, K; Sinn, P.; Pikoſky, A. An integrated model of fixational eye movements and microsaccades. *Proc. Natl. Acad. Sci. U.S.A.* **2011**, *108*, E765-E770.
- [20] Herrmann, C. J. J.; Metzler, R.; Engbert, R. A self-avoiding walk with neural delays as a model of fixational eye movements. *Sci. Rep.* **2017**, *7*, 12958.
- [21] Malkiel, B. G. A random walk down wall street: including a life-cycle guide to personal investing. W. Norton & Co:



- New York, 1999.
- [22] Plerou, V.; Gopikrishnan, P.; Amaral, L. A. N.; Gabaix, X.; Stanley, H. E. Economic fluctuations and anomalous diffusion. *Phys. Rev. E* **2000**, *62*, R3023.
- [23] Fernández, R.; Fröhlich, J.; Sokal, A. D. Random walks, critical phenomena, and triviality in quantum field theory. Springer Science & Business Media: Berlin, 2013.
- [24] Anderson, J. B. Quantum chemistry by random walk.  $H^2P$ ,  $H^+{}_3D_{3h}$   $^1A'_1$ ,  $H_2$   $^3\Sigma^+_u$ ,  $H_4$   $^1\Sigma^+_g$ ,  $Be$   $^1S$ . *J. Chem. Phys.* **1976**, *65*, 4121-4127.
- [25] Lüdtke, O.; Roberts, B. W.; Trautwein, U.; Nagy, G. A random walk down university avenue: life paths, life events, and personality trait change at the transition to university life. *J. Pers. Soc. Psychol.* **2011**, *101*, 620.
- [26] Bouchaud, J.-P.; Potters, M. Theory of financial risk and derivative pricing: from statistical physics to risk management. Cambridge University Press: Cambridge, 2003.
- [27] Pearson, K. The problem of the random walk. *Nature* **1905**, *72*, 294.
- [28] Mises, R. V. Fundamentalsätze der Wahrscheinlichkeitsrechnung. *Math. Z.* **1919**, *4*, 1-97.
- [29] Montroll E. W.; Weiss, G. H. Random walks on lattices. II. *J. Math. Phys.* **1965**, *6*, 167-181.
- [30] Van Kampen, N. G. Stochastic processes in chemistry and physics. Elsevier, 1992.
- [31] Lévy, P. Processus stochastiques et mouvement brownien. Gauthier-Villars: Paris, 1948.
- [32] Hughes, B. D. Random walks and random environments. Oxford University Press: Oxford, 1995.
- [33] Einstein, A. Über die von der molekularkinetischen Theorie der Wärme geforderte Bewegung von in ruhenden Flüssigkeiten suspendierten Teilchen. *Ann. Phys.* **1905**, *322*, 549-560.
- [34] Von Smoluchowski, M. Zur kinetischen Theorie der Brownschen Molekularbewegung und der Suspensionen. *Ann. Phys.* **1906**, *326*, 756-780.
- [35] Sutherland, W. A dynamical theory of diffusion for non-electrolytes and the molecular mass of albumin. *Philos. Mag.* **1905**, *9*, 781-785.
- [36] Langevin, P. Sur la théorie du mouvement brownien. *C. R. Acad. Sci. (Paris)* **1908**, *146*, 530-533.
- [37] Bouchaud, J.-P.; Georges, A. Anomalous diffusion in disordered media: statistical mechanisms, models and physical applications. *Phys. Rep.* **1990**, *195*, 127-293.
- [38] Metzler, R.; Klafter, J. The random walk's guide to anomalous diffusion: a fractional dynamics approach. *Phys. Rep.* **2000**, *339*, 1-77.
- [39] Golding, I.; Cox, E. C. Physical nature of bacterial cytoplasm. *Phys. Rev. Lett.* **2006**, *96*, 098102.
- [40] Manzo, C.; Torreno-Pina, J. A.; Massignan, P.; Lapeyre Jr., G. J.; Lewenstein, M.; Parajo, M. F. G. Weak ergodicity breaking of receptor motion in living cells stemming from random diffusivity. *Phys. Rev. X* **2015**, *5*, 011021.
- [41] Krapf, D.; Lukat, N.; Marinari, E.; Metzler, R.; Oshanin, G.; Selhuber-Unkel, C.; Selhuber-Unkel, A.; Stadler, L.; Weiss, M.; Xu; X. Spectral content of a single non-Brownian trajectory. *Phys. Rev. X* **2019**, *9*, 011019.
- [42] Stadler, L.; Weiss, M. Non-equilibrium forces drive the anomalous diffusion of telomeres in the nucleus of mammalian cells. *New J. Phys.* **2017**, *19*, 113048.
- [43] Kindermann, F.; Dechant, A.; Hohmann, M.; Lausch, T.; Mayer, D.; Schmidt, F.; Lutz, E.; Widera, A. Non-ergodic diffusion of single atoms in a periodic potential. *Nat. Phys.* **2017**, *13*, 137-141.
- [44] Sokolov, I. M. Models of anomalous diffusion in crowded environments. *Soft Matter* **2012**, *8*, 9043-9052.
- [45] Saxton, M. J. Anomalous diffusion due to obstacles: a Monte Carlo study. *Biophys. J.* **1994**, *66*, 394-401.
- [46] Saxton, M. J. Anomalous subdiffusion in fluorescence photobleaching recovery: a monte carlo study. *Biophys. J.* **2001**, *81*, 2226-2240.
- [47] Burov, S.; Jeon, J. H.; Metzler, R.; Barkai, E. Single particle tracking in systems showing anomalous diffusion: the role of weak ergodicity breaking. *Phys. Chem. Chem. Phys.* **2011**, *13*, 1800-1812.
- [48] Ernst, D.; Köhler, J.; Weiss, M. Probing the type of anomalous diffusion with single-particle tracking. *Phys. Chem. Chem. Phys.* **2014**, *16*, 7686-7691.
- [49] Bodrova, A.; Chechkin, A. V.; Cherstvy, A. G.; Metzler, R. Quantifying non-ergodic dynamics of force-free granular gases. *Phys. Chem. Chem. Phys.* **2015**, *17*, 21791-21798.
- [50] Bodrova, A.; Chechkin, A. V.; Cherstvy, A. G.; Safdari, H.; Sokolov, I. M.; Metzler, R. Underdamped scaled Brownian motion: (non-)existence of the overdamped limit in anomalous diffusion. *Sci. Rep.* **2016**, *6*, 30520.
- [51] Lim, S. C.; Muniandy, S. V. Self-similar Gaussian processes for modeling anomalous diffusion. *Phys. Rev. E* **2002**, *66*, 021114.
- [52] Jeon, J.-H.; Chechkin, A. V.; Metzler, R. Scaled Brownian motion: a paradoxical process with a time dependent diffusivity for the description of anomalous diffusion. *Phys. Chem. Chem. Phys.* **2014**, *16*, 15811-15817.
- [53] Mandelbrot, B. B.; Van Ness, J. W. Fractional Brownian motions, fractional noises and applications. *SIAM Rev.* **1968**, *10*, 422-437.
- [54] Metzler, R.; Jeon, J. H.; Cherstvy, A. G.; Barkai, E. Anomalous diffusion models and their properties: non-stationarity, non-ergodicity, and ageing at the centenary of single particle tracking. *Phys. Chem. Chem. Phys.* **2014**, *16*, 24128-24164.
- [55] Marcone, B.; Nampoothiri, S.; Orlandini, E.; Seno, F.; Baldovin, F. Brownian non-Gaussian diffusion of self-avoiding walks. *J. Phys. A* **2022**, *55*, 354003.
- [56] Hegde, A. S.; Chandrashekar, C. M. Characterization of anomalous diffusion in one-dimensional quantum walks. *J. Phys. A* **2022**, *55*, 234006.
- [57] Vitali, S.; Paradisi, P.; Pagnini, G. Anomalous diffusion originated by two Markovian hopping-trap mechanisms. *J. Phys. A* **2022**, *55*, 224012.
- [58] Sabzikar, F.; Kabala, J.; Burnecki, K.; Tempered fractionally integrated process with stable noise as a transient anomalous diffusion model. *J. Phys. A* **2022**, *55*, 174002.
- [59] Wang, W.; Cherstvy, A. G.; Chechkin, A. V.; Thapa, S.; Seno, F.; Liu, X.; Metzler, R. Fractional Brownian motion with random diffusivity: emerging residual non-ergodicity below the correlation time. *J. Phys. A* **2020**, *53*, 474001.
- [60] Hughes, B. D.; Shlesinger, M. F.; Montroll, E. W. Random walks with self-similar clusters. *Proc. Natl. Acad. Sci. U.S.A.* **1981**, *78*, 3287-3291.
- [61] Weissman, H.; Weiss, G. H.; Havlin, S. Transport properties of the continuous-time random walk with a long-tailed waiting-time density. *J. Stat. Phys.* **1989**, *57*, 301-317.
- [62] Lévy, P. Théorie de l'addition des variables aléatoires. Gauthier-Villars: Paris, 1937.

- [63] Chechkin, A. V.; Metzler, R.; Klafter, J.; Gonchar, V. Y. Introduction to the theory of Lévy flights. In *Anomalous Transport: Foundations and Applications*; Klages, R.; Radons, G.; Sokolov, I. M., Eds.; Springer: Berlin, 2008; pp 129-162.
- [64] Shlesinger, M. F.; Klafter, J. Lévy walks versus Lévy flights, on growth and form. Springer: Dordrecht, 1986.
- [65] Zaburdaev, V.; Denisov, S.; Klafter, J. Lévy walks. *Rev. Mod. Phys.* **2015**, *87*, 483.
- [66] Magdziarz, M.; Zorawik, T. Limit properties of Lévy walks. *J. Phys. A* **2020**, *53*, .
- [67] Massignan, P.; Manzo, C.; Torreno-Pina, J. A.; García-Parajo, M. F.; Lewenstein, M.; Lapeyre Jr., G. J. Nonergodic subdiffusion from Brownian motion in an inhomogeneous medium. *Phys. Rev. Lett.* **2014**, *112*, 150603.
- [68] Meroz, Y.; Sokolov, I. M. A toolbox for determining subdiffusive mechanisms. *Phys. Rep.* **2015**, *573*, 1-29.
- [69] Makarava, N.; Benmehdi, S.; Holschneider, M. Bayesian estimation of self-similarity exponent. *Phys. Rev. E* **2011**, *84*, 021109.
- [70] Metzler, R.; Tejedor, V.; Jeon, J. H.; He, Y.; Deng, W. H.; Burov, S.; Barkai, E. Analysis of single particle trajectories: from normal to anomalous diffusion. *Acta Phys. Pol. B* **2009**, *40*.
- [71] Magdziarz, M.; Weron, A.; Burnecki, K.; Klafter, J. Fractional Brownian motion versus the continuous-time random walk: a simple test for subdiffusive dynamics. *Phys. Rev. Lett.* **2009**, *103*, 180602.
- [72] Metzler, R. Brownian motion and beyond: first-passage, power spectrum, non-Gaussianity, and anomalous diffusion. *J. Stat. Mech.* **2019**, *2019*, 114003.
- [73] Vilk, O.; Aghion, E.; Nathan, R.; Toledo, S.; Metzler, R.; Assaf, M. Classification of anomalous diffusion in animal movement data using power spectral analysis. *J. Phys. A* **2022**, *55*, 334004.
- [74] Sposini, V.; Krapf, D.; Marinari, E.; et al., Towards a robust criterion of anomalous diffusion. *Commun. Phys.* **2022**, *5*, 305.
- [75] Condamin, S.; Bénichou, O.; Tejedor, V.; Voituriez, R.; Klafter, J. First-passage times in complex scale-invariant media. *Nature* **2007**, *450*, 77-80.
- [76] Slezak, J.; Metzler, R.; Magdziarz, M. Codifference can detect ergodicity breaking and non-Gaussianity. *New J. Phys.* **2019**, *21*, 053008.
- [77] Maraj, K.; Szarek, D.; Sikora, G.; Wyłomańska, A. Empirical anomaly measure for finite-variance processes. *J. Phys. A* **2020**, *54*, 024001.
- [78] Chen, L.; Bassler, K. E.; McCauley, J. L.; Gunaratne, G. H. Anomalous scaling of stochastic processes and the Moses effect. *Phys. Rev. E* **2017**, *95*, 042141.
- [79] Martin, D. S.; Forstner, M. B.; Käs, J. A. Apparent subdiffusion inherent to single particle tracking. *Biophys. J.* **2002**, *83*, 2109-2117.
- [80] Prezhdo, O. V. Advancing physical chemistry with machine learning. *J. Phys. Chem. Lett.* **2020**, *11*, 9656-9658.
- [81] Back, S.; Yoon, J.; Tian, N.; Zhong, W.; Tran, K.; Ulissi, Z. W. Convolutional neural network of atomic surface structures to predict binding energies for high-throughput screening of catalysts. *J. Phys. Chem. Lett.* **2019**, *10*, 4401-4408.
- [82] Batra, R.; Chan, H.; Kamath, G.; Ramprasad, R.; Cherukara, M. J.; Sankaranarayanan, S. Screening of therapeutic agents for COVID-19 using machine learning and ensemble docking studies. *J. Phys. Chem. Lett.*, **2020**, *11*, 7058-7065.
- [83] Dral, P. O. Quantum chemistry in the age of machine learning. *J. Phys. Chem. Lett.* **2020**, *11*, 2336-2347.
- [84] Granik, N.; Weiss, L. E.; Nehme, E.; Levin, M.; Chein, M.; Perlson, E.; Roichman, Y.; Shechtman, Y. Single-particle diffusion characterization by deep learning. *Biophys. J.* **2019**, *117*, 185-192.
- [85] Bo, S.; Schmidt, F.; Eichhorn, R.; Volpe, G. Measurement of anomalous diffusion using recurrent neural networks. *Phys. Rev. E* **2019**, *100*, 010102.
- [86] Muñoz-Gil, G.; Garcia-March, M. A.; Manzo, C.; Martín-Guerrero, J. D.; Lewenstein, M. Single trajectory characterization via machine learning. *New J. Phys.* **2020**, *22*, 013010.
- [87] Muñoz-Gil, G.; Volpe, G.; García-March, M. A.; Metzler, R.; Lewenstein, M.; Manzo, C. The anomalous diffusion challenge: single trajectory characterisation as a competition. In *Emerging Topics in Artificial Intelligence 2020*, Vol. 11469. SPIE, 2020.
- [88] Manzo, C.; Muñoz-Gil, G.; Volpe, G.; Garcia-March, M. A.; Lewenstein, M.; Metzler, R. Preface: Characterisation of physical processes from anomalous diffusion data. *J. Phys. A* **2023**, *56*, 010401.
- [89] Gajowczyk, M.; Szwabiński, J. Detection of anomalous diffusion with deep residual networks. *Entropy* **2021**, *23*, 649.
- [90] Burnecki, K.; Weron, A. Fractional Lévy stable motion can model subdiffusive dynamics. *Phys. Rev. E* **2010**, *82*, 021130.
- [91] Loch-Olszewska, H.; Szwabiński, J. Impact of feature choice on machine learning classification of fractional anomalous diffusion. *Entropy* **2020**, *22*, 1436.
- [92] Jeon, J.-H.; Barkai, E.; Metzler, R. Noisy continuous time random walks. *J. Chem. Phys.* **2013**, *139*, 121916.
- [93] Mandelbrot B. B.; Wallis, J. R. Noah, Joseph, and operational hydrology. *Water Resour. Res.* **1968**, *4*, 909-918.
- [94] Aghion, E.; Meyer, P. G.; Adlakh, V.; Kantz, H.; Bassler, K. E. Moses, Noah and Joseph effects in Lévy walks. *New J. Phys.* **2021**, *23*, 023002.
- [95] Meyer, P. G.; Aghion, E.; Kantz, H. Decomposing the effect of anomalous diffusion enables direct calculation of the Hurst exponent and model classification for single random paths. *J. Phys. A* **2022**, *55*, 274001.
- [96] Thapa, S.; Lomholt, M. A.; Krog, J.; Cherstvy, A. G.; Metzler, R. Bayesian analysis of single-particle tracking data using the nested-sampling algorithm: maximum-likelihood model selection applied to stochastic-diffusivity data. *Phys. Chem. Chem. Phys.* **2018**, *20*, 29018-29037.
- [97] Park, S.; Thapa, S.; Kim, Y.; Lomholt, M. A.; Jeon, J.-H. Bayesian inference of Lévy walks via hidden Markov models. *J. Phys. A* **2021**, *54*, 484001.
- [98] Szegedy, C.; Zaremba, W.; Sutskever, I.; Bruna, J.; Erhan, D.; Goodfellow, I.; Fergus, R. Intriguing properties of neural networks. In *2nd International Conference on Learning Representations, ICLR 2014*.
- [99] Kowalek, P.; Loch-Olszewska, H.; Szwabiński, J. Classification of diffusion modes in single-particle tracking data: feature-based versus deep-learning approach. *Phys. Rev. E* **2019**, *100*, 032410.
- [100] Muñoz-Gil, G.; Volpe, G.; García-March, M. A.; et al. Objective comparison of methods to decode anomalous diffusion. *Nat. Commun.* **2021**, *12*, 6253.
- [101] Argun, A.; Volpe, G.; Bo, S. Classification, inference

- and segmentation of anomalous diffusion with recurrent neural networks. *J. Phys. A* **2021**, *54*, 294003.
- [102] Garibo-i-Orts, Ò.; Baeza-Bosca, A.; Garcia-March, A.; Conejero, J. A. Efficient recurrent neural network methods for anomalously diffusing single particle short and noisy trajectories. *J. Phys. A* **2021**, *54*, 504002.
- [103] Li, D.; Yao, Q.; Huang, Z. WaveNet-based deep neural networks for the characterization of anomalous diffusion (WADNet). *J. Phys. A* **2021**, *54*, 404003.
- [104] Firbas, N.; Garibo-i-Orts, Ò.; Garcia-March, M. Á.; Conejero, J. A. Characterization of anomalous diffusion through convolutional transformers. *J. Phys. A* **2023**, *56*, 014001.
- [105] AL-hada, E. A.; Tang, X.; Deng, W. Classification of stochastic processes by convolutional neural networks. *J. Phys. A* **2022**, *55*, 274006.
- [106] Gentili A.; Volpe, G. Characterization of anomalous diffusion classical statistics powered by deep learning (CONDOR). *J. Phys. A* **2021**, *54*, 314003,
- [107] Manzo, C. Extreme learning machine for the characterization of anomalous diffusion from single trajectories (andi-elm). *J. Phys. A* **2021**, *54*, 334002.
- [108] Kowalek, P.; Loch-Olszewska, H.; Łaszczuk, Ł.; Opała, J.; Szwabiński, J. Boosting the performance of anomalous diffusion classifiers with the proper choice of features. *J. Phys. A* **2022**, *55*, 244005.
- [109] Pinholt, H. D.; Bohr, S. S. R.; Iversen, J. F.; Boomsma, W.; Hatzakis, N. S. Single-particle diffusional fingerprinting: a machine-learning framework for quantitative analysis of heterogeneous diffusion. *Proc. Natl. Acad. Sci. U.S.A.* **2021**, *118*, e2104624118.
- [110] Seckler, H.; Metzler, R. Bayesian deep learning for error estimation in the analysis of anomalous diffusion. *Nat. Commun.* **2022**, *13* 6717.
- [111] Thapa, S.; Park, S.; Kim, Y.; Jeon, J. H.; Metzler, R.; Lomholt, M. A. Bayesian inference of scaled versus fractional Brownian motion. *J. Phys. A* **2022**, *55*, 194003.
- [112] Muñoz-Gil, G.; Requena, B.; Volpe, G.; Garcia-March, M.A.; Manzo, C. *AnDiChallenge/ANDI\_datasets: Challenge 2020 release (v.1.0)*, <https://doi.org/10.5281/zenodo.4775311>, (accessed 2023-07-24).
- [113] Krog, J.; Jacobsen, L. H.; Lund, F. W.; Wüstner, D.; Lomholt, M. A. Bayesian model selection with fractional Brownian motion. *J. Stat. Mech.* **2018**, *2018*, 093501.
- [114] Janczura, J.; Kowalek, P.; Loch-Olszewska, H.; Szwabiński, J.; Weron, A. Classification of particle trajectories in living cells: machine learning versus statistical testing hypothesis for fractional anomalous diffusion. *Phys. Rev. E* **2020**, *102*, 032402.
- [115] Verdier, H.; Duval, M.; Laurent, F.; Cassé, A.; Vestergaard, C. L.; Masson, J. B. Learning physical properties of anomalous random walks using graph neural networks. *J. Phys. A* **2021**, *54*, 234001.
- [116] Verdier, H.; Laurent, F.; Cassé, A.; Vestergaard, C. L.; Masson, J. B. Variational inference of fractional Brownian motion with linear computational complexity. *Phys. Rev. E* **2022**, *106*, 055311.
- [117] LeCun, Y.; Bengio, Y.; Hinton, G. Deep learning. *Nature* **2015**, *521*, 436-444.
- [118] Chen, Z; Geffroy, L.; Biteen, J. nobias: Analyzing anomalous diffusion in single-molecule tracks with non-parametric Bayesian inference. *Front. Bioinform.* **2021**, *1*, 742073.
- [119] Fukushima, K. neocognitron: A self-organizing neural network model for a mechanism of pattern recognition unaffected by shift in position. *Biol. Cybern.* **1980**, *36*, 193-202.
- [120] Hochreiter S.; Schmidhuber, J. Long short-term memory. *Neural Comput.* **1997**, *9*, 1735-1780.
- [121] Kiureghian A.; Ditlevsen, O. Aleatory or epistemic? Does it matter?. *Structural Safety* **2009**, *31*, 105-112.
- [122] Kendall, A.; Gal, Y. What uncertainties do we need in Bayesian deep learning for computer vision?. *Adv. Neural Inf. Process. Syst.* **2017**, *30*, 5580-5590.
- [123] Wang, Q.; Ma, Y.; Zhao, K.; Tian, Y. A comprehensive survey of loss functions in machine learning. *Ann. Data Sci.* **2022**, *9*, 1-26.
- [124] Nix, D. A.; Weigend, A. S. Estimating the mean and variance of the target probability distribution. In *Proc. 1994 IEEE Int. Conf. Neural Networks (ICNN'94)*, Vol. 1. IEEE, 1994.
- [125] Kolmogorov, A. N.; Foundations of the theory of probability. Chelsea Publishing Co.: London, 1950.
- [126] Metropolis, N.; Ulam, S. The Monte Carlo method. *J. Am. Stat. Assoc.* **1949**, *44*, 335-34.
- [127] Binder, K.; Monte Carlo methods in statistical physics. Springer: Berlin, 1986.
- [128] Lakshminarayanan, B.; Pritzel, A.; Blundell, C. Simple and scalable predictive uncertainty estimation using deep ensembles. *Adv. Neural Inf. Process. Syst.* **2017**, *30*.
- [129] Gal, Y.; Ghahramani, Z. Dropout as a Bayesian approximation: representing model uncertainty in deep learning. In *Int. Conf. Machine Learning* PMLR, 2016.
- [130] Gal, Y. Uncertainty in deep learning. Doctoral dissertation. (Cambridge University: Cambridge, 2016).
- [131] Maddox, W. J.; Izmailov, P.; Garipov, T.; Vetrov, D. P.; Wilson, A. G. A simple baseline for Bayesian uncertainty in deep learning. *Adv. Neural Inf. Process. Syst.* **2019**, *32*.
- [132] Wilson, A. G.; Izmailov, P. Bayesian deep learning and a probabilistic perspective of generalization. *Adv. Neural Inf. Process. Syst.* **2020**, *33*, 4697-4708.
- [133] Bottou, L. Large-scale machine learning with stochastic gradient descent. In *Proceedings of COMPSTAT'2010: 19th International Conference on Computational Statistics Paris France, August 22-27, 2010 Keynote, Invited and Contributed Papers*. Physica-Verlag HD, 2010, 177-186.
- [134] Naeini, M. P.; Cooper, G.; Hauskrecht, M. Obtaining well calibrated probabilities using Bayesian binning. In *Proceedings of the AAAI conference on artificial intelligence*. Vol. 29. No. 1. 2015.
- [135] Levi, D.; Gispan, L.; Giladi, N.; Fetaya, E. Evaluating and calibrating uncertainty prediction in regression tasks. *Sensors* **2022**, *22*, 5540.
- [136] Doerries, T. J.; Checkin, A. V.; Metzler, R. Apparent anomalous diffusion and non-Gaussian distributions in a simple mobile-immobile transport model with Poissonian switching. *J. R. Soc. Interface* **2022**, *19*, 20220233.
- [137] Van Genuchten, M. T.; Wierenga, P. J. Mass transfer studies in sorbing porous media I. analytical solutions. *Soil Sci. Soc. Am. J.* **1976**, *40*, 473-480.
- [138] Deans, H. H. A mathematical model for dispersion in the direction of flow of porous media. *Soc. Pet. Eng. J.* **1963**, *3*, 49-52.
- [139] Wagner, T.; Kroll, A.; Haramagatti, C. R.; Lipinski, H.-G.; Wiemann, M. Classification and segmentation of

- nanoparticle diffusion trajectories in cellular micro environments. *PLoS ONE* **2017**, *12*, e0170165.
- [140] Weron A.; Janczura, J.; Boryczka, E.; Sungkaworn, T.; Calebiro, D. Statistical testing approach for fractional anomalous diffusion classification. *Phys. Rev. E* **2019**, *99*, 042149.
- [141] James, G.; Witten, D.; Hastie, T.; Tibshirani, R. An introduction to statistical learning with applications in R. Springer: New York, 2013.
- [142] Song, Y.-Y.; LU, Y. Decision tree methods: applications for classification and prediction., *Shanghai Archives of Psychiatry* **2015**, *27*, 130.
- [143] Meyer, P. G.; Metzler, R. Stochastic processes in a confining harmonic potential in the presence of static and dynamic measurement noise. *New J. Phys.* **2023**, *25*, 063003
- [144] Schütz, G. M.; Trimper, S. Elephants can always remember: Exact long-range memory effects in a non-Markovian random walk. *Phys. Rev. E* **2004**, *70*, 045101.
- [145] Mangalam, M.; Metzler, R.; Kelty-Stephen, D. G. Ergodic characterization of non-ergodic anomalous diffusion processes. *Phys. Rev. Res.* **2023**, *5*, 023144.
- [146] Malinin, A.; Prokhorenkova, L.; Ustimenko, A. Uncertainty in gradient boosting via ensembles. International Conference on Learning Representations **2020**; E-print arXiv:2006.10562.
- [147] Requena, B.; Masó, S.; Bertran, J.; Lewenstein, M.; Manzo, C.; Muñoz-Gil, G. Inferring pointwise diffusion properties of single trajectories with deep learning. arXiv:2302.00410 (2023).
- [148] Martinez, Q.; Chen, C.; Xia, J.; Bahai, H. Sequence-to-sequence change-point detection in single-particle trajectories via recurrent neural network for measuring self-diffusion. *Transp. Porous Media* **2023**, *147*, 679-701.
- [149] Muñoz-Gil, G.; i Corominas, G. G.; Lewenstein, M. Unsupervised learning of anomalous diffusion data: an anomaly detection approach. *J. Phys. A* **2021**, *54*, 504001.
- [150] Garibo-i-Orts, Ò.; Firbas, N.; Sebastiá, L.; Conejero, J. A. Gramian angular fields for leveraging pretrained computer vision models with anomalous diffusion trajectories. *Phys. Rev. E* **2023**, *3*, 034138.
- [151] Wang, Z.; Oates, T. Imaging time-series to improve classification and imputation. In *Proceedings of the 24th International Conference on Artificial Intelligence*. 2015.
- [152] Eckmann, J.-P.; Oliffson Kamphorst, S.; Ruelle, D. Recurrence plots of dynamical systems. *EPL* **1987**, *4*, 973.



# Supplementary Material: Machine-Learning Solutions for the Analysis of Single-Particle Diffusion Trajectories

Henrik Seckler,<sup>1</sup> Janusz Szwabiński,<sup>2</sup> and Ralf Metzler<sup>1,3</sup>

<sup>1</sup>*Institute for Physics & Astronomy, University of Potsdam, 14476 Potsdam-Golm, Germany*

<sup>2</sup>*Hugo Steinhaus Center, Faculty of Pure and Applied Mathematics, Wrocław University of Science and Technology, Wybrzeże Wyspiańskiego 27, 50-370 Wrocław, Poland* <sup>3</sup>*Asia Pacific Centre for Theoretical Physics, Pohang 37673, Republic of Korea*

## Appendix A: Anomalous Diffusion Models

We here provide a brief primer on the considered anomalous diffusion models.

*CTRW.* The continuous-time random walk (CTRW) is defined as a random walk, in which the times between jumps and the spatial displacements are stochastic variables [1–3]. In our case, we are considering a CTRW for which the waiting time density  $\psi(\tau)$  features a power law tail,  $\psi(\tau) \simeq \tau^{-1-\alpha}$  with scaling exponent  $0 < \alpha < 1$ . Thus the characteristic waiting time diverges,  $\int_0^\infty \tau\psi(\tau)d\tau = \infty$ . The spatial displacements follow a Gaussian law.

*LW.* The Lévy walk (LW) is a special case of a CTRW. As above we consider power-law distributed waiting times,  $\psi(\tau) \simeq \tau^{-1-\sigma}$ , but the displacements are correlated, such that the walker always moves with constant speed  $v$  in one direction for one waiting time, randomly choosing a new direction after each waiting time. One can show that this leads to an anomalous diffusion exponent  $\alpha$  given by [4]

$$\alpha = \begin{cases} 2 & \text{if } 0 < \sigma < 1 \text{ (ballistic diffusion)} \\ 3 - \sigma & \text{if } 1 < \sigma < 2 \text{ (superdiffusion)}. \end{cases} \quad (\text{A1})$$

*FBM.* Fractional Brownian motion (FBM) is characterized by long-range, power-law correlations between the increments. It is created by fractional Gaussian noise for the increments, given by

$$\langle \xi_{fGn}(t)\xi_{fGn}(t + \tau) \rangle \sim \alpha(\alpha - 1)K_\alpha\tau^{\alpha-2} \quad (\text{A2})$$

for sufficiently large  $\tau$ , where  $\alpha$  is the anomalous diffusion exponent and  $K_\alpha$  is the generalised diffusion constant [5].

*SBM.* Scaled Brownian motion (SBM) features the time dependent diffusivity  $K(t) = \alpha K_\alpha t^{\alpha-1}$ , equivalent to the Langevin equation

$$\frac{dx(t)}{dt} = \sqrt{2K(t)}\xi(t), \quad (\text{A3})$$

where  $\xi(t)$  is white, zero-mean Gaussian noise [6].

*ATTM.* Similar to SBM, the annealed transient time motion (ATTM) features a diffusion coefficient  $D$  varying over time. But in contrast to SBM, the change in diffusivity is random in magnitude and occurs instantaneously in a manner similar to the jumps in a CTRW. Here we consider diffusion coefficients sampled from the density  $P(D) \simeq D^{\sigma-1}$  and use a delta-distributed waiting times  $P(\tau) \propto \delta(\tau - D^{-\gamma})$ , with  $\sigma < \gamma < \sigma + 1$ . As shown in [7], this leads to subdiffusion with  $\alpha = \sigma/\gamma$ .

## Appendix B: Trajectory characteristics

In this appendix, the definitions of the features listed in table 1 are briefly introduced.

### 1. Original features

#### a. Anomalous exponent

Four estimates for the anomalous diffusion exponent  $\alpha$  were used as separate features:

1. the standard estimation, based on fitting the empirical TAMSD to equation (2),

2. 3 estimation methods proposed for trajectories with noise, which is normally-distributed with zero mean [8],

(a) using the estimator

$$\hat{\alpha} = \frac{n_{\max} \sum_{n=1}^{n_{\max}} \ln(n) \ln(\langle \mathbf{r}^2(n\Delta t) \rangle) - \sum_{n=1}^{n_{\max}} \ln(n) \left( \sum_{n=1}^{n_{\max}} \ln(\langle \mathbf{r}^2(n\Delta t) \rangle) \right)}{n_{\max} \sum_{n=1}^{n_{\max}} \ln^2(n) - \left( \sum_{n=1}^{n_{\max}} \ln(n) \right)^2}, \quad (\text{B1})$$

with  $n_{\max}$  equal to 0.1 times the trajectory length, rounded to the nearest lower integer (but not less than 4),

(b) simultaneous fitting of the parameters  $\hat{D}$ ,  $\hat{\alpha}$ , and  $\hat{\sigma}$  in the relation

$$\langle \mathbf{r}^2(t) \rangle = 2d\hat{D}t^{\hat{\alpha}} + \hat{\sigma}^2, \quad (\text{B2})$$

where  $d$  denotes the embedding dimension,  $D$  is the diffusion coefficient, and  $\sigma^2$  is the variance of noise,

(c) simultaneous fitting of the parameters  $\hat{D}$  and  $\hat{\alpha}$  in the equation

$$\langle \mathbf{r}^2(n\Delta t) \rangle = 2d\hat{D}(\Delta t)^{\hat{\alpha}}(n^{\hat{\alpha}} - 1). \quad (\text{B3})$$

#### b. Diffusion coefficient

An estimator of the diffusion coefficient was extracted from the fit of the empirical TAMSD to equation (2).

#### c. Asymmetry

The asymmetry is defined as

$$A = -\log \left( 1 - \frac{(\lambda_1 - \lambda_2)^2}{2(\lambda_1 + \lambda_2)} \right), \quad (\text{B4})$$

where  $\lambda_1$  and  $\lambda_2$  are the eigenvalues of the tensor of gyration [9]. For a 2D random walk of  $N$  steps, the tensor is given by

$$\mathbf{T} = \begin{pmatrix} \frac{1}{N+1} \sum_{j=0}^N (x_j - \langle x \rangle)^2 & \frac{1}{N+1} \sum_{j=0}^N (x_j - \langle x \rangle)(y_j - \langle y \rangle) \\ \frac{1}{N+1} \sum_{j=0}^N (x_j - \langle x \rangle)(y_j - \langle y \rangle) & \frac{1}{N+1} \sum_{j=0}^N (y_j - \langle y \rangle)^2 \end{pmatrix}, \quad (\text{B5})$$

where  $\langle x \rangle = (1/[N+1]) \sum_{j=0}^N x_j$  is the average of the  $x$  coordinate over all steps in the random walk. The asymmetry is expected to help to detect directed motion.

#### d. Efficiency

The efficiency  $E$  relates the net squared displacement of a particle to the sum of squared step lengths,

$$E = \frac{|X_N - X_0|^2}{N \sum_{i=1}^N |X_i - X_{i-1}|^2}. \quad (\text{B6})$$

Similarly to the asymmetry, it may help to detect directed motion.

#### e. Empirical velocity autocorrelation function

The empirical velocity autocorrelation function [10] for lag 1 and point  $n$  is defined as

$$\chi_n = \frac{1}{N-n} \sum_{i=0}^{N-1-n} (X_{i+1+n} - X_{i+n})(X_{i+1} - X_i). \quad (\text{B7})$$

It can be used to distinguish different subdiffusion processes. In [11],  $\chi_n$  for points  $n = 1$  and  $n = 2$  was used.

*f. Fractal dimension*

The fractal dimension is a measure of the space-filling capacity of a pattern (a trajectory in our case). For a planar trajectory, it may be calculated as

$$D_f = \frac{\ln N}{\ln(NdL^{-1})}, \quad (\text{B8})$$

where  $L$  is the total length of the trajectory,  $N$  is the number of steps, and  $d$  is the largest distance between any two positions [12]. It usually takes values around 1 for directed motion, around 2 for normal diffusion. For subdiffusive CTRW it is also around 2, while for FBM it is larger than 2.

*g. Maximal excursion*

The maximal excursion of the particle is given by the formula

$$\text{ME} = \frac{\max(|X_{i+1} - X_i|)}{X_N - X_0} \quad (\text{B9})$$

It detects relatively long jumps (in comparison to the overall displacement).

*h. Mean maximal excursion*

The mean maximal excursion can replace the MSD as the observable used to determine the anomalous diffusion exponent [13]. It is defined as the standardized value of the largest distance traveled by a particle,

$$T_n = \frac{\max(|X_i - X_0|)}{\sqrt{\hat{\sigma}_N^2(t_N - t_0)}}. \quad (\text{B10})$$

The parameter  $\hat{\sigma}_N$  is a consistent estimator of the standard deviation,

$$\hat{\sigma}_N^2 = \frac{1}{2N\Delta t} \sum_{j=1}^N \|X_j - X_{j-1}\|_2^2. \quad (\text{B11})$$

*i. Mean Gaussianity*

The Gaussianity  $g(n)$  checks the Gaussian statistics of increments of a trajectory [14] and is defined as

$$g(n) = \frac{2\langle r_n^4 \rangle}{3\langle r_n^2 \rangle^2} - 1, \quad (\text{B12})$$

where  $\langle r_n^k \rangle$  denotes the  $k$ th moment of the trajectory at time lag  $n$ . The Gaussianity for normal diffusion is equal to 0. The same result should be obtained for FBM, since its increments follow a Gaussian distribution. Other types of motion should show deviations from that value.

Instead of looking at Gaussianities at single time lags, in [11] the mean Gaussianity over all lags was used as one of the features,

$$\langle g \rangle = \frac{1}{N} \sum_{i=1}^N g(n). \quad (\text{B13})$$

*j. Mean-squared displacement ratio*

The MSD ratio gives information about the shape of the corresponding MSD curve. We will define it as

$$\text{MSDR}(n_1, n_2) = \frac{\langle r_{n_1}^2 \rangle}{\langle r_{n_2}^2 \rangle} - \frac{n_1}{n_2}, \quad (\text{B14})$$

where  $n_1 < n_2$ .  $MSDR = 0$  is zero for normal diffusion ( $\alpha = 1$ ). We should get  $MSDR \leq 0$  for sub- and  $MSDR \geq 0$  for superdiffusion. In [11],  $n_2 = n_1 + \Delta t$  was taken and then the averaged ratio over all  $n_1 = 1, 2, \dots, N - 1$  was calculated for every trajectory.

#### k. Kurtosis

The Kurtosis gives insight into the asymmetry and peakedness of the distribution of points within a trajectory [15]. It is defined as the the fourth moment,

$$K = \frac{1}{N} \sum_{i=1}^N \frac{(x_i^p - \bar{x}^p)^4}{\sigma_{x^p}^4}, \quad (\text{B15})$$

of the projection of the position vectors  $X_i$  onto the dominant eigenvector  $\vec{r}$  of the gyration tensor (B5),

$$x_i^p = X_i \cdot \vec{r}. \quad (\text{B16})$$

Here,  $\bar{x}^p$  is the mean projected position and  $\sigma_{x^p}$  the standard deviation of  $x^p$ .

#### l. Statistics based on $p$ -variation

The empirical  $p$ -variation is given by the formula [16]

$$V_m^{(p)} = \sum_{k=0}^{\frac{N}{m}-1} |X_{(k+1)m} - X_{km}|^p \propto km^{\gamma^p}. \quad (\text{B17})$$

This statistic can be used to detect fractional Lévy stable motion (including FBM). Six features based on  $V_m^{(p)}$  were used for the classification of trajectories:

1. the power  $\gamma^p$  fitted to  $p$ -variation for lags 1 to 5,
2. the statistic  $P$  used in [17], based on the monotonicity changes of  $V_m^{(p)}$  as a function of  $m$ :

$$P = \begin{cases} 0 & \text{if } V_m^{(p)} \text{ does not change the monotonicity,} \\ 1 & \text{if } V_m^{(p)} \text{ is convex for the highest } p \text{ for which it is not monotonous,} \\ -1 & \text{if } V_m^{(p)} \text{ is concave for the highest } p \text{ for which it is not monotonous.} \end{cases} \quad (\text{B18})$$

#### m. Straightness

The straightness  $S$  measures the average direction change between subsequent steps. It relates the net displacement of a particle to the sum of all step lengths,

$$S = \frac{|X_N - X_0|}{\sum_{i=1}^N |X_i - X_{i-1}|}. \quad (\text{B19})$$

#### n. Trappedness

The trappedness is understood as the probability that a diffusing particle is trapped in a bounded region with radius  $r_0$  up to some observation time  $t$ . Saxton [9] estimated this probability with

$$P(D, t, r_0) = 10^{0.2048 - 2.5117(Dt/r_0^2)}. \quad (\text{B20})$$

In the above expression,  $r_0$  is approximated by half of the maximum distance between any two positions along a given trajectory and  $D$  is estimated by fitting the first two points of the MSD curve (i.e., it is the so called short-time diffusion coefficient).



## 2. Additional features

### a. D'Agostino-Pearson test statistic

The d'Agostino-Pearson  $\kappa^2$  test statistic [18] measures the departure of a given sample from normality. It is defined as

$$\kappa^2 = Z_1(g_1) + Z_2(K), \quad (\text{B21})$$

where  $K$  is the sample kurtosis given by equation (B15) and  $g_1 = m_3/m_2^{3/2}$  is the sample skewness with  $m_j$  being the  $j$ th sample central moment. The transformations  $Z_1$  and  $Z_2$  should bring the distributions of the skewness and kurtosis as close to the standard normal as possible. This feature helps to distinguish ATTM and SBM from other motions.

### b. Kolmogorov-Smirnov statistic against $\chi^2$ distribution

The Kolmogorov-Smirnov statistic quantifies the distance between the empirical distribution function of the sample  $F_n(X)$  and the cumulative distribution function  $G_n(X)$  of a reference distribution,

$$D_n = \sup_X |F_n(X) - G_n(X)|. \quad (\text{B22})$$

Here,  $n$  is the number of observations (i.e., the length of a trajectory). The value of this statistic for the empirical distribution of squared increments of a trajectory against the sampled  $\chi^2$  distribution has been taken as the next feature. The rationale of such choice is that for a Gaussian trajectory the theoretical distribution of squared increments is the mentioned  $\chi^2$  distribution.

### c. Noah, Moses, and Joseph exponents

For processes with stationary increments, there are in principle two mechanisms that violate the Gaussian central limit theorem and produce anomalous scaling of MSD: long-time increment correlations (referred to as the Joseph effect) or a flat-tailed increment distribution (the Noah effect) [19]. FBM is the prototypical process that exhibits the first effect and LW the latter one. An anomalous scaling can also be induced by a non-stationary increment distribution [19]. In this case, we talk about the Moses effect. It should help to handle ATTM and SBM trajectories.

All three effects may be quantified by exponents, which can be used as features. Given a stochastic process  $X_t$  and the corresponding increment process  $\delta_t(\tau) = X_{t+\tau} - X_t$ , the Joseph, Moses and Noah exponents are defined as follows:

1. The Joseph exponent  $J$  is estimated from the ensemble average of the rescaled range statistic,

$$E \left[ \frac{\max_{1 \leq s \leq t} [X_s - \frac{s}{t} X_t] - \min_{1 \leq s \leq t} [X_s - \frac{s}{t} X_t]}{\sigma_t} \right] \sim t^J, \quad (\text{B23})$$

where  $\sigma_t$  is the standard deviation of the process  $X_t$ .

2. The Moses exponent  $M$  is determined from the scaling of the ensemble probability distribution of the sum of the absolute value of the increments which can be estimated by the scaling of the median of the probability distribution of  $Y_t = \sum_{s=0}^{t-1} |\delta_s|$ ,

$$E[Y_t] \sim t^{M+\frac{1}{2}}. \quad (\text{B24})$$

3. The Noah exponent  $L$  is extracted from the scaling of the ensemble probability distribution of the sum of increment squares, which can be estimated by the scaling of the median of the probability distribution of  $Z_t = \sum_{s=0}^{t-1} \delta_s^2$ :

$$E[Z_t] \sim t^{2L+2M-1}. \quad (\text{B25})$$

*d. Detrending moving average*

The detrending moving average (DMA) statistic [20] is given by

$$DMA(\tau) = \frac{1}{N - \tau + 1} \sum_{i=\tau}^N \left( X_i - \overline{X}_i^\tau \right)^2, \quad (\text{B26})$$

for  $\tau = 1, 2, \dots$ , where  $\overline{X}_i^\tau$  is a moving average of  $\tau$  observations, i.e.,  $\overline{X}_i^\tau = \frac{1}{\tau+1} \sum_{j=0}^{\tau} X_{i-j}$ . According to [20], a DMA-based statistical test can help in the detection of the scaled Brownian motion. In [11],  $DMA(1)$  and  $DMA(2)$  were used as features.

*e. Average moving window characteristics*

Let us define the following moving window characteristic

$$MW = \frac{1}{2(N - m - 1)} \sum_{t=1}^{N-m-1} \left| \text{sgn} \left( \overline{X}_{t+1}^{(m)} - \overline{X}_t^{(m)} \right) - \text{sgn} \left( \overline{X}_t^{(m)} - \overline{X}_{t-1}^{(m)} \right) \right|, \quad (\text{B27})$$

where  $\overline{X}^{(m)}$  denotes a statistic of the process calculated within the window of length  $m$  and  $\text{sgn}$  is the sign function. In [11], eight attributes based on the above formula have been used:

1. the mean and the standard deviation for  $\overline{X}$  with windows of lengths  $m = 10$  and  $m = 20$ ,
2. the  $MW$  with the same window lengths calculated separately for  $x$  and  $y$  coordinates.

*f. Maximum standard deviation*

The last two features used in [11] are based on the standard deviation  $\sigma_m$  of the process calculated within a window of length  $m$ . They are given by

$$MXM = \frac{\max(\sigma_m(t))}{\min(\sigma_m(t))} \quad (\text{B28})$$

and

$$MXC = \frac{\max|\sigma_m(t+1) - \sigma_m(t)|}{\sigma}, \quad (\text{B29})$$

where  $\sigma$  denotes the overall standard deviation of the sample. A window of length  $m = 3$  was used and the features were calculated for both coordinates separately. They should improve the detection of ATTM type of movements.

## Appendix C: Supplementary Figures

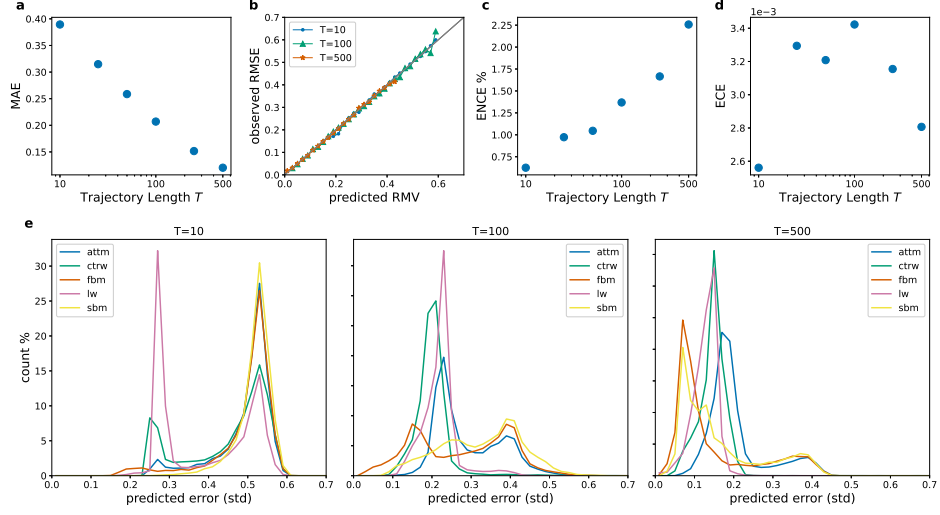


FIG. S1: Results, as presented in [21], for the regression of the anomalous diffusion exponent with included error estimation. The figure shows (a) the regression performance via the mean absolute error in dependence of the trajectory length, (b) the reliability diagram, where coinciding predicted and observed error is represented as the diagonal, (c) the expected normalized (or unnormalized in (d)) calibration error, and (e) the predicted error distribution, for different trajectory length split depending on ground truth models. The distribution of errors in (e) has been extensively analyzed in [21], where it was used to gain insights into the learning process of the machine. For each trajectory length, the shown results were obtained from a test dataset of  $10^5$  trajectories, using a model trained on  $10^6$  trajectories of random models and exponents.

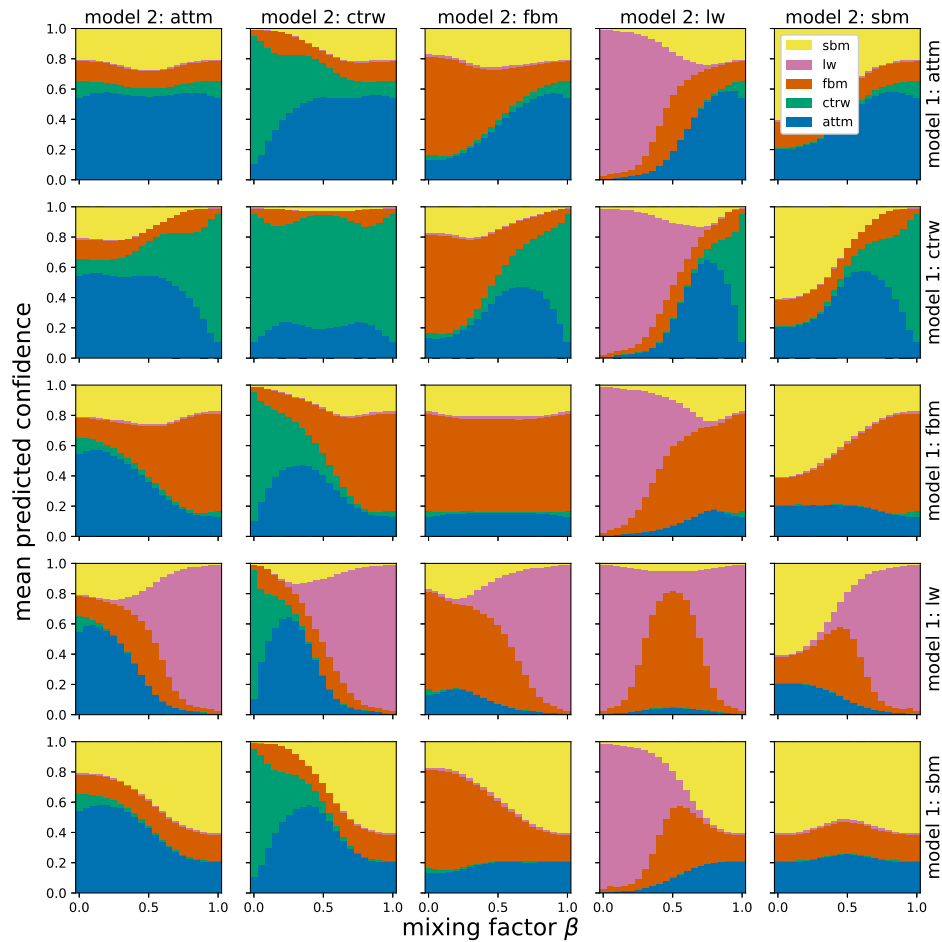


FIG. S2: Classification for a superposition of 2 models in 1D. The figure depicts the mean confidence assigned by the neural network, when given a mixture of two models in dependence of the superposition factor. The depicted results are obtained from 1D trajectories with 100 data points each.

- 
- [1] Montroll E. W.; Weiss, G. H. Random walks on lattices. II. *J. Math. Phys.* **1965**, *6*, 167-181.
- [2] Hughes, B. D.; Shlesinger, M. F.; Montroll, E. W. Random walks with self-similar clusters. *Proc. Natl. Acad. Sci. U.S.A.* **1981**, *78*, 3287-3291.
- [3] Weissman, H.; Weiss, G. H.; Havlin, S. Transport properties of the continuous-time random walk with a long-tailed waiting-time density. *J. Stat. Phys.* **1989**, *57*, 301-317.
- [4] Zaburdaev, V.; Denisov, S.; Klafter, J. Lévy walks. *Rev. Mod. Phys.* **2015**, *87*, 483.
- [5] Mandelbrot, B. B.; Van Ness, J. W. Fractional Brownian motions, fractional noises and applications. *SIAM Rev.* **1968**, *10*, 422-437.
- [6] Jeon, J.-H.; Chechkin, A. V.; Metzler, R. Scaled Brownian motion: a paradoxical process with a time dependent diffusivity for the description of anomalous diffusion. *Phys. Chem. Chem. Phys.* **2014**, *16*, 15811-15817.
- [7] Massignan, P.; Manzo, C.; Torreno-Pina, J. A.; García-Parajo, M. F.; Lewenstein, M.; Lapeyre Jr., G. J. Nonergodic subdiffusion from Brownian motion in an inhomogeneous medium. *Phys. Rev. Lett.* **2014**, *112*, 150603.
- [8] Lanoiselée, Y.; Sikora, G.; Grzesiek, A.; Grebenkov, D. S.; Wyłomańska, A. Optimal parameters for anomalous-diffusion-exponent estimation from noisy data. *Phys. Rev. E* **2018**, *98*, 062139.
- [9] Saxton, M. J. Lateral diffusion in an archipelago. single-particle diffusion. *Biophys. J.* **1993**, *64*, 1766-1780.
- [10] Weber, S. C.; Spakowitz, A. J.; Theriot, J. A. Bacterial chromosomal loci move subdiffusively through a viscoelastic cytoplasm. *Phys. Rev. Lett.* **2010**, *104*, 238102.
- [11] Kowalek, P.; Loch-Olszewska, H.; Łaszczuk, Ł.; Opała, J.; Szwabiński, J. Boosting the performance of anomalous diffusion classifiers with the proper choice of features. *J. Phys. A* **2022**, *55*, 244005.
- [12] Katz, M. J.; George, E. B. Fractals and the analysis of growth paths. *Bull. Math. Biol.* **1985**, *47*, 273-286.

- [13] Tejedor, V.; Bénichou, O.; Voituriez, R.; Jungmann, R.; Simmel, F.; Selhuber-Unkel, C.; Oddershede, L. B.; Metzler, R. Quantitative analysis of single particle trajectories: mean maximal excursion method. *Biophys. J.* **2010**, *98*, 1364-1372.
- [14] Ernst, D.; Köhler, J.; Weiss, M. Probing the type of anomalous diffusion with single-particle tracking. *Phys. Chem. Chem. Phys.* **2014**, *16*, 7686-7691.
- [15] Helmuth, J. A.; Burckhardt, C. J.; Koumoutsakos, P.; Greber, U. F.; Sbalzarini, I. F. A novel supervised trajectory segmentation algorithm identifies distinct types of human adenovirus motion in host cells. *J. Struct. Biol.* **2007**, *159*, 347-358.
- [16] Burnecki, K.; Weron, A. Fractional Lévy stable motion can model subdiffusive dynamics. *Phys. Rev. E* **2010**, *82*, 021130.
- [17] Loch-Olszewska, H.; Szwabiński, J. Impact of feature choice on machine learning classification of fractional anomalous diffusion. *Entropy* **2020**, *22*, 1436.
- [18] D'Agostino, R.; Pearson, E. S. Tests for departure from normality. Empirical results for the distributions of  $b_2$  and  $\sqrt{b_1}$ . *Biometrika* **1973**, *60*, 613-622.
- [19] Aghion, E.; Meyer, P. G.; Adlakha, V.; Kantz, H.; Bassler, K. E. Moses, Noah and Joseph effects in Lévy walks. *New J. Phys.* **2021**, *23*, 023002.
- [20] Balcerek, M.; Burnecki, K.; Sikora, G.; Wyłomańska, A. Discriminating Gaussian processes via quadratic form statistics. *Chaos* **2021**, *31*, 063101.
- [21] Seckler, H.; Metzler, R. Bayesian deep learning for error estimation in the analysis of anomalous diffusion. *Nat. Commun.* **2022**, *13*, 6717.